GLUCOSE TRANSPORTER EXPRESSION IN LUNG GRANULOMAS FROM MYCOBACTERIUM TUBERCULOSIS-INFECTED MONKEYS

by

Hong Liu

BS Biology, Iowa State University, 2013

Submitted to the Graduate Faculty of

the Department of Infectious Diseases and Microbiology

Graduate School of Public Health in partial fulfillment

of the requirements for the degree of

Master of Science

University of Pittsburgh

2017

UNIVERSITY OF PITTSBURGH

Graduate School of Public Health

This thesis was presented

by

Hong Liu

It was defended on

April 20, 2017

and approved by

Thesis advisor:
Joshua T. Mattila, PhD
Assistant Professor
Infectious Diseases and Microbiology
Graduate School of Public Health
University of Pittsburgh

Committee Members:

Robbie B. Mailliard, PhD
Assistant Professor and Director of the MS Program
Infectious Diseases and Microbiology
Graduate School of Public Health
University of Pittsburgh

Dexing Zeng, Ph.D.
Professor, Molecular Imaging Laboratory
School of Medicine
Department of Radiology
University of Pittsburgh

Joshua T. Mattila, PhD

GLUCOSE TRANSPORTER EXPRESSION IN LUNG GRANULOMAS FROM *MYCOBACTERIUM TUBERCULOSIS*-INFECTED MONKEYS

Hong Liu, MS

University of Pittsburgh, 2017

ABSTRACT

Tuberculosis (TB) remains a major threat to public health that causes tremendous morbidity and mortality in developing countries. The diagnostic tests for TB have problems with sensitivity, specificity, and ability to measure treatment outcomes. Positron emission tomography/computed tomography (PET/CT) imaging techniques can provide a fast and sensitive way of diagnosing active TB and can be a valuable tool of studying TB-associated inflammation in tissues. The most common PET probe is FDG, a glucose analog that is taken up by metabolically active cells, but the factors driving FDG uptake and the cells responsible for this in granulomas remain unknown. Our study focused on expression of glucose transporters (Gluts), a diverse set of proteins involved in glucose metabolism, in granulomas from *Mycobacterium tuberculosis*-infected monkeys. Our objective was to measure Glut expression, localization, and cellular source. We used RT-PCR and multi-color immunohistochemistry to accomplish this objective. We found that there was substantial variation in Glut expression between granulomas and uninfected lung, and that expression of individual Gluts did not correlate with FDG uptake in tissues. Our immunohistochemical studies demonstrated that Glut1 and 3 were strongly expressed by epithelioid macrophages, a cell type that exists in hypoxic environments and is likely to be using glycolysis to generate energy. We also identified a correlation

between neutrophils and FDG uptake, suggesting these cells may contribute to PET/CT-measured inflammation in granulomas. Our results suggest that multiple factors, rather than a single Glut, drive FDG uptake in granulomas, but also indicate Glut expression on specific cell populations may strongly influence PET/CT detection of TB. Future work identifying the relationship between these cell populations and changes in FDG uptake over the course of disease may lead to important new information on pathogenesis in TB. Public health significance of our study may provide new insight and perspective of metabolic and physiological characteristics in granuloma and potentially improve the sensitivity and usefulness of existing PET/CT imaging technique.

TABLE OF CONTENTS

LIST OF TABLES

LIST OF FIGURES

PREFACE

I would like to thank my advisor and a true friend Dr. Joshua Mattila for all the support he gave me throughout the project. He is the most wonderful person I have ever known. He gave me the new strength and confidence to work my way up after I hit the bottom because of unsuccessful experiments. He has been nice, patient and thoughtful to me ever since. I am so glad to have him as my advisor and friend. Then, I would also like to thank our lab manager, Beth Junecko for all the lab skills and assistance she provided. She is such a meticulous and organized person, I have learned more than just lab skills but also her spirits. I also want to thank my committee members Dr. Robbie Milliard and Dr. Zeng for their suggestions and assistance with my thesis. Thank you to all the members who provided samples and help from Dr. Flynn's lab. Lastly, thank for all my family and friends for their love and support.

1.0 INTRODUCTION

1.1 TUBERCULOSIS

1.1.1 Epidemiology

Tuberculosis (TB) is caused by the intracellular pathogen *Mycobacterium tuberculosis* (Mtb). Mtb is an aerobic, acid-fast bacterium that has a thick cell walls and complex outer membrane that enable them to survive in harsh environmental condition and infect host cells (1). TB is one of the oldest human diseases and even with modern medicine humankind still suffers tremendous losses from this ancient disease. According to the WHO, it is estimated nearly 2 billion people, or one third of world's populations is infected with Mtb. In 2015, TB killed 1.4 million people and there were 10.4 million develop active disease (2). HIV-infected individuals are as significant and there were 400,000 deaths among the 1.2 million people who are co-infected. In this population, the risk of getting active TB disease increases from 10% lifetime risk to 10% each year, which is 20 times higher than HIV non-infected people (3, 4). Besides those infected with HIV, people from all age groups are at risk of developing TB, but those who smoke or have medical conditions are at higher risk than others. (5)

The greatest incidence of TB occurs in the developing countries in Asia and Africa. Six countries include India, Indonesia, China, Nigeria, Pakistan and South Africa account for 60% of total cases (2). Despite the considerable amount effort and resource spent to curb the spread of TB, many developing countries still face enormous disease burdens. Many reasons may contribute to this outcome including poor public health infrastructure, limited prevention measures, low socioeconomic status, and delayed diagnosis and treatment among others.

Bacillus Calmette-Guérin (BCG) is the only vaccine developed through the serial in vitro passage of *M. bovis* and it was widely used in TB endemic areas. The vaccine has been shown to protect children from severe manifestations of TB such as TB meningitis or disseminated infection (6). However, in countries like India, the vaccine efficacy varied in different populations and some received no protection at all (7-9). The efficiency of BCG vaccine is still under investigation and new vaccine development is stumbled due to complex disease pathology within host and maintain efficacy from preclinical model to human challenge model (10). Therefore, there is still a long way to go in the battle between humans and Mtb.

1.1.2 Pathogenesis and Clinical Manifestation

The life cycle of Mtb starts when a person inhales air droplets that contain infectious bacteria. Once a bacterium gets into the lung, it is phagocytized by an alveolar macrophage. Mtb can resist macrophage killing by interfering the phagosome-lysosome acidification pathway and inhibit innate immune functions (11, 12). This allows it to persist and replicate intracellularly, eventually causing cell death and necrosis. Release of

bacterial products and cellular components leads to recruitment of additional Mtb host cells including macrophages, monocytes, and neutrophils, furthering the infection. Adaptive immunity is delayed in TB (13) and recruitment of lymphocytes to the site of infection take place at between weeks 3-5 post infection which initiates granuloma formation (14, 15). Granulomas are organized structures composed of cluster of immune cells which participate in bacteria killing and cytokine production to contain the bacteria from escaping (6, 16). The factors that lead to containment of infection or progression to disease are not fully understood, but it is believed a balance between bacteria killing and control of pathology is crucial to maintain the integrity and function of a granuloma (17, 18)

Macrophage polarization is a key factor that determines the fate of the granuloma. Once activated, macrophage can differentiate into either M1 (classically activated macrophages) or M2 (alternatively activated macrophage) (19, 20). Several factors may affect the balance of M1 and M2 polarization in granulomas including microbial factors, cell-to-cell contact with T cells, and others are currently under investigation (18). M1 macrophages are pro-inflammatory and are required for killing bacteria. In response to interferon-γ (IFN-γ) from Th1 cells and toll-like receptor (TLR) ligands such as lipopolysaccharide (LPS), these cells produce proinflammatory cytokines including TNF and IL-12, and chemokines that recruit and activate T cells and killing bacteria (11, 18, 21, 22). M2 macrophages are anti-inflammatory in nature. In response to Th2 cytokines IL-13 and IL-4, they produce IL-10, TGF-β and IL-6 that downregulate Th1 response and prevent tissue damage (11, 18, 19, 22). Therefore, an extreme number of M1 macrophages may cause too much inflammation and pathology, while too few may lead

to an ineffective killing of the bacteria. A similar balance needs to be achieved for M2 macrophage where too many, or too few, will inhibit bacterial containment and protection.

As for neutrophils, the role they play in early TB infection is still controversial. However, several studies have shown replicating bacteria in neutrophils derived from TB patients, and neutrophil-induced inflammation being associated with poorly control of TB, suggesting that neutrophils may contribute to increase disease pathology and bacteria dissemination at late stage of infection (6, 16, 23). Hence, the key factor in determining if a granuloma can function properly to effectively contain the bacteria may be the balance between inflammation and tissue repair at the granuloma site.

Although the physical characteristics of granulomas occur over a spectrum, there are four commonly-found types. The most commonly considered granuloma is the necrotic (caseous) granuloma. This granuloma type has a distinct caseous center surround by macrophages and outer lymphocyte cuff. Other types of granuloma include non-necrotic granulomas that are like caseous granulomas but do not have the necrotic center, suppurative granuloma where the caseum is dominated by neutrophils and fibrotic granulomas, which are composed of calcified regions that are associated with successful immune response and fewer inflammatory cells (16, 18). Patients who have active TB may have more than one type of granuloma found in the lung (24) but condition of an individual granuloma won't provide enough information about the disease condition and risk of dissemination. A system wide review of the pathology include the number and types of granulomas present and disease burden assessment may help determine the risk of disease dissemination for patient who have active disease or disease reactivation for patients who have latent infection.

TB is often classified as active or latent based on its clinical manifestation. Active disease is described as when a person experiences symptoms associated with TB include coughing, pain in the chest, fever, weight lost, fatigue and night sweat (25). People who develop active disease can transmit bacteria when they speak, breath or cough and healthy people can become infected when they inhale bacteria-containing droplet nuclei (26). Latently infected people are asymptotic and not do not transmit the bacteria. Usually, the immune system does a good job keeping the infection in check, and 90% of the people who become infected develop latent infections that never progress to symptomatic TB. However, there is 10% lifetime risk for developing reactivation TB, and the risk may increase if people are immunosuppressed, smoking, malnourished, alcohol abusers, in renal failure, or have diabetes and cancers (2, 27). There is a 45% chance of mortality for individuals with active TB if they don't get proper treatment in time (27).

1.1.3 Diagnosis and treatment

The conventional method of detecting active TB is based on clinical signs and symptoms, sputum test and chest x-ray. However, these techniques suffer from poor sensitivity (40-80%) and this limitation can make diagnosing TB difficult, thereby delaying time to treatment. Chest x-ray is used to detect abnormal lung structure such as cavities and infiltrations but the results are operator dependent and sometimes give rise to nonspecific results that are not sufficient to generate a definite diagnosis. Culture-based sputum tests take 2-8 weeks for the results to be available and require multiple samples. Microscopy-based sputum tests are more rapid but the low sensitivity and efficiency of microscopic detection of acid-fast stained bacteria limit this technique. Moreover, it can

be difficult to get sputum from children, a population that is at high risk for TB. Immunological tests such as Tuberculin Skin Test (TST) and Interferon Gamma Release Assay (IGRA) may give rise to false positive and false negative results and neither of them can differentiate latent infection and active disease (3, 28-30). Hence, a new tool is strongly needed to improve the diagnosis efficiency.

Treatment of active TB requires a rigorous six month multiple drug regimen which include rifampicin, isoniazid and others. However, drug resistance is an increasingly severe problem for curing TB due because many patients have difficulty adhering to the long-term therapy and poor outcomes are associated with treating MDR-TB (31). Most anti-TB drugs are decades old, and although several new drugs are under development, with lack of complete understanding of the complex disease pathology and effective means of assessing treatment responses have made developing successful new drug challenging.

1.2 PET/CT IMAGING

1.2.1 Application

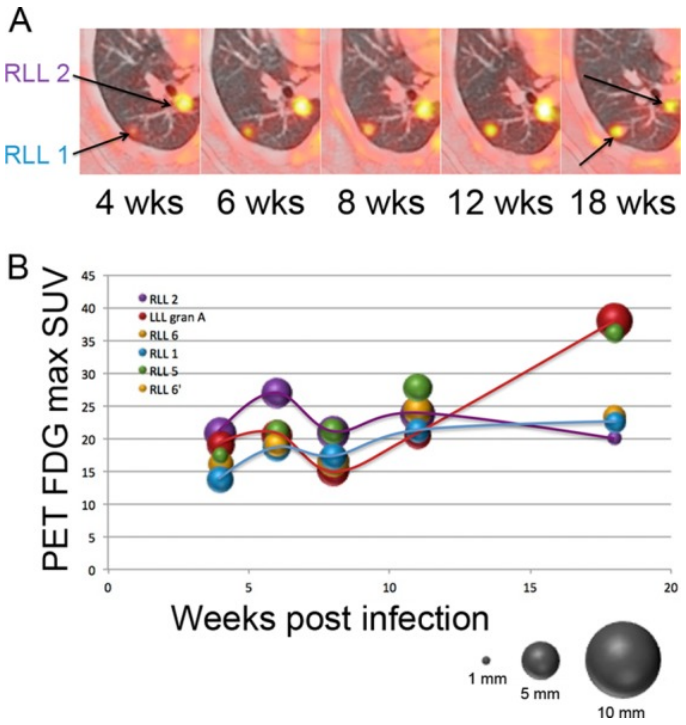

Figure 1. Lung granulomas are dynamic and independent

(A). Changes of size and metabolic activity shown in yellow from two granulomas at right lower lobe (RLL) at different time post infection. **(B)**. Change of granuloma size and metabolic activity shown as SUV from multiple granulomas at different time post infection. Lin et. al. 2013. Radiologic responses in cynomolgous macaques for assessing tuberculosis chemotherapy regimens.

Positron emission tomography (PET) and computed tomography (CT) is well established as a tool for cancer diagnosis and research and recently it has been used for TB diagnosis and research (28). The principle of PET/CT is based on the detecting a radiolabeled probe and overlaying this image with a high-resolution x-ray image to show anatomic features (32). 18F-fluorodeoxyglucose (18F-FDG) is a glucose analog

radioactive tracer that's commonly used to detect TB pathology and inflammation. It is taken up by metabolically active cells, and the amount of uptake can be quantified and described as a Standard Uptake Unit (SUV) (31). In TB, granulomas are indicated as 'hot' bright areas, where the higher the inflammation, the brighter the granuloma's SUV (33) (Figure 1A). By reviewing the overall PET/CT signal and clinical test results, physicians can assess the extent of the disease and offer a more effective course of treatment.

As for research, PET/CT provides another means for studying the complex pathophysiological response to TB over the full spectrum of disease. This is application, PET/CT studies of nonhuman primates are particularly valuable because monkeys infected with Mtb develop similar types of lesions, disease pathology and clinical manifestation as human (33-35). This model system has been of great value and has uncovered new aspects of TB, including how lesions are dynamic over time and independent from one another in the same host, possibly increasing in size and inflammation where other granulomas can go the opposite way (Figure 1B) (24, 33). Moreover, when combined with other tests, PET/CT can be used to predict drug response, which can become a useful tool for monitoring the efficacy of new drugs (28, 33).

1.3 FACTORS CONTRIBUTING TO PET/CT SIGNAL

1.3.1 The Warburg effect as the basis of 18F-FDG PET

The Warburg effect describes the phenomenon where cells shift to aerobic glycolysis rather than mitochondrial oxidative phosphorylation, and often occurs under hypoxic conditions (11). This metabolic strategy is commonly seen in cancer cells and activated immune cells in granuloma tissue that use glycolysis to produce ATP more rapidly than normal metabolic pathways would allow (11). This permits rapid cell growth, proliferation, and cellular biosynthetic capacity, and for immune cells this supports rapid inflammatory responses and effective immune functions (11, 36, 37). Since FDG uptake is influenced by the cell mediated inflammation and other factors, we may suggest there is a link between FDG uptake and successfully induced Warburg effect. The Warburg effect is mediated, in part, by hypoxia inducible factor (HIF-1) which can be induced by pro-inflammatory cytokines, growth factors, and infections (11, 36, 38-43). HIF-1 plays a variety of roles in the activation of genes (36, 44) important for maintaining tissue integrity and homeostasis under hypoxia environment, which is an induced environment with depleted oxygen and nutrients. While hypoxic environments can limit bacteria spread and infection, it may also cause tissue damage (11, 45). In addition, HIF-1 also play important roles in TH17 T cell differentiation (11, 46), activation, regulation of glycolytic capacity in myeloid cells (11, 44), and production of pro-inflammatory cytokines and Warburg-effect enzymes in dendritic cells (11, 47). Hence, this suggests that under the influence from Warburg effect, a number of genes and cells can be activated to play essential roles to promoting inflammation and immune response. This can lead to an increase in cellular

activity and energy demand for activated immune cells, which give rise to the high glucose uptake and PET/CT signal.

Cell mediated inflammation is one important factor that may contribute to PET/CT signal change (48, 49), and the variation in the number of inflammatory cells including activated macrophages and neutrophils can be used as a criteria to measure the change. We therefore speculate that granulomas with a high SUV may contain a large number of inflammatory cells.

1.3.2 Glucose Transporters

Inflammatory cell 18F-FDG uptake is mediated by glucose transporters, and their expression level could be one important factor contributing to changes in PET/CT signal. The facilitative glucose transporter family (Glut) mediates glucose uptake in cells (50). There are 14 Glut isoforms and structurally they all have 12 transmembrane-spanning alpha helices and a single N-linked oligosaccharide (50). Based on their sequence similarity, GLUTs can be categorized into 3 classes. Briefly, Class I Gluts (Glut1-4 and Glut14, which is a gene duplication of Glut3) are well characterized classic glucose transporters that transport glucose but not fructose. Class II Gluts (Glut5, 7, 9 and 11) which mainly transport fructose but Glut7, 9 and 11 have high affinity for glucose but don't not transporter 2-DG, a glucose analogue. Class III Gluts (Glut6, 8, 10, 12 and 13), which share structure similarities with their N-glycosylation side at the fifth extracellular loop rather than at first loop seen in Class I and II glucose transporters. In addition, class III Gluts contain intracellular localization signals that are not found in class I and II glucose

transporters and these Gluts are retained intracellularly under steady state conditions rather than localizing to membranes (50, 51).

Every glucose transporter is different from each other in terms of their tissue-specific distribution, affinity to glucose or fructose, and other featured functions. For example, Glut1 is the major glucose transporter responsible for most of the glucose metabolism in the body. It is ubiquitously expressed in erythrocyte membranes and in the blood tissue barrier, but can also be found at high levels in brain, eye, peripheral nerve, placenta, and certain cancer cells (50, 52). Glut 2 on the other hand is mainly found in liver, kidney and intestine epithelial cells located in the basolateral membrane. It is also found in the brain, pancreatic β-cells, and hypothalamus where it provides glucose-sensing functions for insulin production (53, 54). Glut3 is a neuron specific glucose transporter, which is mainly expressed in brain and nerve cells but can also be found in testis, placenta, lymphocytes, monocytes/macrophages, and platelets (50, 51, 55). Glut4 is an insulin-regulated transporter which play important role in glucose transport in insulin sensitive tissues such as brown and white adipose tissue, skeletal and cardiac muscle. Under insulin stimulation, Glut4 translocate from the intracellular location to the cell surface, result in dramatically increase of glucose transporter activity. Therefore, impaired Glut4 translocation is linked to insulin resistance and diabetes (50, 51, 56). Glut5 does not have transport ability for glucose but fructose. It is found in intestinal epithelial cells, kidney proximal tubules and germinal cells of testis (50, 57). As for Glut6, it predominately expressed in the brain, spleen, and peripheral leucocytes and may play major role of glucose transport in leucocyte (50, 58). The rest of the glucose transporters are less well

studies compared to the ones just listed. Detailed feature of all glucose transporters can be found on table 1.

Several studies have shown that Gluts are upregulated in cancer cells, where the Warburg effect drives increased glycolytic activity (57, 59, 60). A similar behavior has been seen in Mtb infection where host metabolism switches to glycolysis to support immune cell activation and proliferation (11). Presumably, this also increases glucose transporters expression in granulomas as well. Shi et, al. (36) demonstrated Glut gene expression in a number of animal studies. In mice that were infected with TB, a 2-fold increase of Glut1 and 3, and a 6-fold increase in Glut6 transcript expression was noted, whereas in Mtb-infected rabbits only Glut4 gene expression was upregulated. They also measured Glut expression in lung granuloma from humans with active TB, and found upregulation of genes encoding Glut1, 3, 5 and 6, with Glut6 being the highest induced (11, 36). These data suggest there is increased Glut expression in TB granuloma and the level of those Gluts expressions may be one key factor give rise to different PET/CT signal.

The immune-pathologic response is complex in granuloma tissue, we believe the study we do may provide more information of cellular and metabolic response in monkey lung TB granulomas and in addition of the links we found between glucose transporter expression pattern and PET/CT signal change which might shed light of finding new PET/CT tracer and improving the diagnosing technique.

Table 1. Summary of the properties of glucose transporter members

GLUT	Affinity Km^2 (mM) for glucose	Site of expression	Main feature
Glut1	5	Erythrocyte and ubiquitous distribution in tissue an culture cells	Basal glucose uptake
Glut2	17	Kidney, pancreas, liver, intestine, brain and bronchus	High capacity and low affinity transporter
Glut3	1.4	Brain, nerve cells, testis, white blood cells	Glucose transport between neurons
Glut4	5	Adipose tissue, skeletal and cardiac muscles	Insulin-regulated transporter in muscle and fat
Glut5	No activity	Intestine, kidney, testis	Transporter of fructose
Glut6	5	Brain, spleen and peripheral leucocytes	Glucose transporter for leucocytes
Glut7	0.3	Small intestine, colon, testis and prostate	High affinity for both glucose and fructose
Glut8	2	Testis, brain, adrenal gland, liver, spleen, brown adipose tissue and lung	Fuel supply for mature spermatozoa, glucose uptake for milk synthesis in mammary gland
Glut9	0.6	Kidney, placenta and liver	May exchange glucose or fructose for urate
Glut10	0.3	Heart, lung, brain, liver, skeletal muscle, pancreas, placenta and kidney	Located at chromosomal region 20q12-13.1 and possible link to type 2 diabetes
Glut11	0.16	Heart, skeletal muscles, kidney, adipose tissue and pancreas	Glucose and fructose transporter in muscle
Glut12	Unknown	Skeletal muscle, heart, small intestine, prostate and mammary gland	Another insulin responsive glucose transporter in muscle
Glut13	No activity	Brain	H+/myo-inositol co-transporter
Glut14	Unknown	Testis	95% identical to Glut3, gene duplication of Glut3

2.0 STATEMENT OF THE PROJECT AND SPECIFIC AIMS

PET/CT imaging provides a tool for studying inflammation and dynamic pathophysiological changes in the lungs of Mtb infected monkeys. Nevertheless, many questions are unanswered regarding mechanisms of FDG uptake by granulomas. We explored the molecular and cellular contribution glucose transporters play in FDG uptake and PET/CT analysis of TB. We hypothesized that inflammation and glucose transporter expression play cardinal roles in granuloma FDG avidity. This study may provide more information on pathologic inflammation in granulomas, and potentially improve current PET/CT imaging techniques.

2.1 AIM 1: ASSESS GLUCOSE TRANSPORTERS EXPRESSION IN GRANULOMAS FROM MTB-INFECTED MONKEYS.

A: Design primers specific for all 14 Glut isomers based on their mRNA sequences and test their effectiveness.

B: Measure Glut expression in monkey granulomas by qRT-PCR

2.2 AIM 2: IDENTIFY THE CELL THAT EXPRESS GLUCOSE TRANSPORTERS AND THEIR LOCALIZATION IN GRANULOMAS.

A: Stain glucose transporters and cellular makers in formalin-fixed paraffin-embedded granuloma sections and identify their expression patterns by microscopy.

B: Use image analysis software to count relevant cell populations and compare granulomas glucose transporters expression.

C: Correlated glucose transporter expression patterns in different granulomas with their FDG uptake (known as SUV) from PET/CT data.

3.0 MATERIALS AND METHODS

3.1 ANIMAL SAMPLES FOR STUDY

The animals in this study were cynomolgus macaques (*Macaca fascicularis*) involved in studies performed by JoAnne Flynn's laboratory at the University of Pittsburgh. Monkeys were infected with low dose of *M. tuberculosi*s under BSL3 conditions and euthanized at predetermined time points. Preliminary pathologic analysis and tissue processing was done by Flynn Lab personnel. We used samples stored at -80C before RNA isolation and qRT-PCR analysis (listed in table 2).

Table 2. List of samples of studies

Monkey, tissue ID	Type	Name
JF11-5, 30	Granuloma	Active granuloma
JF-13-15A, 18	Granuloma	Active granuloma
JF10-63, 10	Granuloma, FFPE	RML gran 2
JF10-63, 12	Granuloma, FFPE	LUL gran 5
JF10-63, 37	Granuloma, FFPE	LLL gran 13
JF10-63, 40	Granuloma, FFPE	LLL gran 16
JF11-1, 17	Granuloma, FFPE	RLL gran 7
JF11-1, 28	Granuloma, FFPE	LUL gran 1
JF11-1, 39	Granuloma, FFPE	LLL gran A
JF11-1, 43	Granuloma, FFPE	LLL gran 6
JF11-2, 16	Granuloma, FFPE	RLL gran 1
JF11-2, 30	Granuloma, FFPE	LUL gran 3
JF11-2 36	Granuloma, FFPE	LML gran 2
JF11-2, 42	Granuloma, FFPE	LLL gran 4
9711 FF2	Granuloma tissue, RNA	LLL gran8
9711 FF3	Normal tissue, RNA	LLL
9711 RL2	Granuloma tissue, RNA	LLL gran16
9811 RL1	Normal tissue, RNA	RML
14812 FF3	Normal tissue, RNA	RML
14812 FF7	Granuloma tissue, RNA	LLL gr11
17211 FF6	Granuloma tissue, RNA	RLL7
17211 FF7	Granuloma tissue, RNA	RLL gran14
17211 RL7	Granuloma tissue, RNA	RLL gran25
20212 FF7	Granuloma tissue, RNA	RLL gran11
20212 FF9	Normal tissue, RNA	RML
20912 FF6	Normal tissue, RNA	LUL
20912 RL5	Granuloma tissue, RNA	LUL gr7
22010 RL1	Granuloma tissue, RNA	Access gr3 (drug treated)
22010 RL3	Granuloma tissue, RNA	Access gr1 consolidation (drug treated)
22010 RL4	Normal tissue, RNA	RLL
22610 FF1	Normal tissue, RNA	LUL
22610 FF2	Normal tissue, RNA	LLL grC
22610 FF3	Normal tissue, RNA	RML
Pooled RNA stock	Multiple granulomas, RNA	NA

3.2 SELECTION OF PRIMERS

We started primer design by locating the glucose transporters mRNA sequences for *Macaca fascicularis* in GenBank. CLC Main Workbench (QIAGEN) was used to align

sequences from multiple variants and to generate consensus sequence for each glucose transporter genes. These consensus sequences were put into Integrated DNA Technologies (Coralville, IA) web primer design tool (available at idtdna.com) and two sets of primer sets with appropriate melting temperatures and predicted product size. A total of 28 forward and reverse primers (100uM) were purchased from Integrated DNA Technologies and 10X (10uM) and 100X (1uM) diluted working stocks were prepared for RT-PCR experiments. RNA was obtained from macaque granulomas by homogenizing the tissue in Trizol (ThermoFisher Scientific, Waltham, MA) with a BeadBeater in BSL3 containment followed by phenol-chloroform isolation. Isolated RNA was treated with DNase (Turbo DNA-free Kit, Invitrogen) before testing the two forward and reverse primer sets by RT-PCR. Complete removal of DNA was confirmed by a no-reverse transcriptase (RT) control sample for each sample in parallel with a reverse transcriptase-positive sample. Initial studies were performed using the pooled RNA harvested from multiple Mtb infected monkey tissues and the primer set had higher performance by gel electrophoresis were selected for future use. HPRT1 primers (Realtimeprimers.com) were used as housekeeping control for expression analysis. A detailed list of the Glut primer information is found in table 7.

3.3 REVERSE TRANSCRIPTION PCR

Reagents for RT-PCR were prepared (Table 4) and standard RT-PCR reaction was conducted according to the protocol on the AccessQuick R, T-PCR product sheet (Promega, Madison, WI). Amplification was performed on a T100 Thermal Cycler (Bio-

Rad, Hercules, CA) with the following program: 95 °C for 5 min, 35 cycles at (95 °C of denaturation for 30 seconds, 50 °C of annealing for 30 seconds and 72 °C for 20 seconds). This is followed by final step of elongation at 72 °C for 3 min and held indefinitely at 12 degree.

Table 3. Materials for RT PCR

Reagents	**Volume**
AccessQuick ™Master Mix, 2X	12.5ul
Pooled RNA template	1ul
Primer working stock (Forward and reverse) 10uM	1ul
Nuclease-free water	10ul
AMV Reverse Transcriptase 5U/ul (Promega)	0.5ul
Total	25ul

3.4 GEL ELECTROPHORESIS

PCR products were confirmed via agarose gel electrophoresis. A 2% gel was prepared started by dissolving 2 grams of UltraPure Agarose powder (Invitrogen, Waltham, MA) in a 100ml 0.5 X TBE buffer followed by 2 min microwave heating, cooling and adding 1ul of Gel red Gel Stain (10000x in water, Biotium, Hayward, CA). The gel was then set in a cast with comb and allowed to solidify. Next, the solidified gel was placed

into a gel electrophoresis tank and submerged by 0.5x TBE buffer. The DNA ladder (1ul 5x diluted 50bp DNA ladder, (New England BioLabs, Ipswich, MA) with 1ul Cyan/Orange loading buffer, (Invitrogen, Carlsbad, CA) and 1ul nuclease-free water) and samples (5ul PCR products with 1ul Cyan/Orange loading buffer, (Invitrogen, Carlsbad, CA)) were then loaded into the gel wells and the reaction was set at 80 voltages for 2 hours. Finally, the DNA products were analyzed under the UV transilluminator (Alpha Innotech, San Leandro, CA) and images saved as TIFF files. Relative intensities for the product's bands was measured with the FIJI build of ImageJ (http://fiji.sc/#download).

3.5 RNA EXTRACTION

Twenty tissue samples (see Table 5) contained granuloma were selected for RNA isolation using the RNeasy FFPE kit (QIAGEN, Hilden, Germany) and followed the manufacturer's instruction. In general, the tissue in Trizol underwent centrifugation, incubation, supernatant transfer, mix with chloroform and once more centrifuge, incubation and supernatant transfer. Then at different time point, Glycoblue (ThermoFisher), isopropanol and 70% ETOH wash were added followed by spin, incubation and removal of supernatant. The sample pellet were left to dry and resuspened with nuclease free water. Then 1ul of RNasin was added and incubated for 1 hour but mixing every 15 min. It was then incubated at 65°C for 15 min. Lastly, the samples were treated with DNase as previously indicated according to the manufacturer's protocol and kept at the -20C until use.

Table 4 Tissues selected for RNA isolation

9711 FF2	Granuloma tissue, RNA	LLL gran8
9711 FF3	Normal tissue, RNA	LLL
9711 RL2	Granuloma tissue, RNA	LLL gran16
9811 RL1	Normal tissue, RNA	RML
14812 FF3	Normal tissue, RNA	RML
14812 FF7	Granuloma tissue, RNA	LLL gr11
17211 FF6	Granuloma tissue, RNA	RLL7
17211 FF7	Granuloma tissue, RNA	RLL gran14
17211 RL7	Granuloma tissue, RNA	RLL gran25
20212 FF7	Granuloma tissue, RNA	RLL gran11
20212 FF9	Normal tissue, RNA	RML
20912 FF6	Normal tissue, RNA	LUL
20912 RL5	Granuloma tissue, RNA	LUL gr7
22010 RL1	Granuloma tissue, RNA	Access gr3 (drug treated)
22010 RL3	Granuloma tissue, RNA	Access gr1 consolidation (drug treated)
22010 RL4	Normal tissue, RNA	RLL
22610 FF1	Normal tissue, RNA	LUL
22610 FF2	Normal tissue, RNA	LLL grC
22610 FF3	Normal tissue, RNA	RML

3.6 TWO-STEP QUANTITATIVE REAL TIME PCR

The cDNA synthesis for 20 purified tissue RNA samples was carried out using the High-Capacity cDNA Reverse Transcription Kits (Applied Biosystems, Foster City, CA) according to the manufacturer's protocol. (see Table 6) The T100 thermal cycler for PCR reaction was set at 25 °C for 10 min, 37 °C for 2 hours followed by 85 °C for 5 min and held at 4 °C indefinitely. The cDNA products were kept at -20C until use.

The qPCR experiment was carried out in a 96-well plate with 8 tissues/plate. Each sample was tested for Glut1, 2, 3, 4, 5, 6, 7, 8, 11, 13, 14 expression with HPRT as a housekeeping control. The reagents were prepared (see Table 7) and loaded in an ABI

Prism 7000 Sequence Detection System thermal cycler (Applied Biosystems, Foster City, CA) by the manufacturer's instruction (Thermo Scientific, Waltham, MA). The program was set at 95 °C for 10 min and then followed by 45 cycles at 95 °C for 15 seconds and 50 °C for 30 seconds. The last dissociation step was set at 95 °C for 15 seconds, 50 °C for 20 seconds and 95 °C for 15 seconds. Data from samples with CT values <40 cycles and with one peak in the dissociation curve (indicating a single product) were used to calculate delta CT values. Delta CT values were obtained and relative expression of glucose transporters were normalized in compare to the expression of HPRT control.

Table 5 cDNA synthesis in RT-PCR

Reagents	**Volume**
RNA template	10ul (less than 2 µg of total RNA per 20-µL reaction)
10X RT Buffer	2ul
10X Random Primers	2ul
25X dNTP Mix (100mM)	0.8ul
MultiScribe Reverse Transcriptase 50U/ul	1ul
Nuclease-free water	4.2ul
Total	20ul

Table 6 Materials for qPCR

Reagents	Volume
Maxima SYBR Green/ROX qPCR Master Mix (2X)	12.5ul
cDNA template	1ul
Primer working stock (1uM)	1ul
Nuclease-free water	10.5ul
Total	25ul

3.7 IMMUNOHISTOCHEMISTRY AND MICROSCOPIC IMAGING

Formalin-fixed paraffin-embedded tissue sections were stained as previously described (9). Briefly, tissue sections were deparaffinized in xylene and ethanol and then heated for 30 min in a 2100 retriever (Prestige Medical, Los Angeles, California) contained antigen retrieve buffer. Tissue sections were blocked with 1% BSA-PBS for 30 min and incubated with diluted primary antibodies cocktails for 1 hour in room temperature. The slides were washed 3 times and incubated with either a biotinylated secondary antibody or fluorochrome-conjugated secondary antibodies cocktails. After 3 more washes, tertiary conjugates of either AlexaFluor594-conjugated Streptavidin or Zenon label-labeled antibodies (Life Technologies, Carlsbad, CA) were applied and incubated for an hour at room temperature or in the refrigerator overnight. Then, after another 3 washes, coverslips were mounted with ProLong Gold Mounting Medium with DAPI (Invitrogen, Carlsbad, CA) and cured for 12 hours at room temperature. Primary

antibodies used: Glut1 (Rabbit polyclonal, 1:100 dilution, ThermoFisher), Glut2 (Clone 199017, 1:100 dilution, R&D System, Minneapolis, MN), Glut3 (Rabbit polyclonal, 1:100 dilution, Novus Biological, Littleton, CO), Glut4 (Clone 3G10A3, 1:200 dilution, Novus Biological), CD11c (Clone 5D11, 1:30 dilution, Leica Biosystems, Wetzlar, Germany), CD163 (Clone 10D6, 1:30 dilution, ThermoFisher), CD20 (Rabbit polyclonal, 1:50 dilution, ThermoFisher), CD3 (Rabbit polyclonal, 1:100, Dako, Glostrup Municipality, Denmark), CD206 (Clone 685645, 1:50, R&D System), Negative control Mouse IgG1 (Mouse polyclonal, Dako), Negative Control Rabbit Immunoglobulin Fraction (Rabbit polyclonal, Dako). Secondary antibodies with Biotin Donkey anti-mouse or anti-rabbit antibodies and fluorochrome-labelled secondary antibodies were purchased from Jackson ImmunoResearch (West Grove, PA). Calprotectin was labelled by Zenon antibody-labelling reagents as tertiary antibody. Streptavidin (ThermoFisher) was used in the end as tertiary or quaternary conjugate.

Granulomas were viewed under 200X magnification with either an Olympus confocal microscope maintained by the University of Pittsburgh's Center for Biologic Imaging or Nikon e1000 epifluorescent microscope with motorized stage in the University of Pittsburgh Department of Infectious Disease and Microbiology. DAPI, red, green and far red (pseudo-blue) channels were acquired for each image, and a different cell population was represented with each channel. All tissues were imaged at the same exposure and microscope settings and saved as ND2 files to ensure they could be compared at same level of equality.

3.8 DATA ANALYSIS

Granuloma-containing areas of tissues were outlined with Nikon Elements (Nikon, Minato, Tokyo, Japan) image analysis to create a region of interest that excluded uninvolved lung tissue. Mean Fluorescent Intensity of TRITC channel in the region of interest was acquired using the measurement feature in the analysis software. The data were exported as Excel-format spreadsheets for analysis. The images saved as ND2 files were saved as either TIFF or JPEG format and exported. They underwent preliminary editing in Photoshop (Abode Systems, San Jose, CA) to help further analysis. Cells were quantified in the region of interest using Nikon Element's measurement feature.

Data of qRT-PCR in the ABI Prism 7000 Sequence Detection System Software were analyzed in 7000 system software exported as an Excel file and analyzed by Prism GraphPad. Statistical tests were performed in Prism, with Mann-Whitney for pairwise comparisons and linear regression for correlations.

4.0 RESULTS

4.1 AIM 1: ASSESS GLUCOSE TRANSPORTERS EXPRESSIONS IN THE GRANULOMA TISSUE FROM MTB INFECTED MONKEYS.

4.1.1 Selection of suitable primers for expression experiment

To study the glucose transporters mRNA expression profile, we first selected two potential forward and reverse primer sets for each of the 14 glucose transporters based on monkey DNA sequences found on GenBank and sequence alignment. The primer sequence information can be found on Table 3. With the help from primer design tool, all primer sequences had 100 amplicon length and met their basic requirement in regard of their GC content, melting temperature and others.

Table 7 List of primer sequences used for RT-PCR analysis

Glut	Forward 1	Reverse 1	Forward 2	Reverse 2	Picked Set
Glut1	CCAGTATGTGGAGCAACTATGT	GTCTCGGGAACTTTGAAGTAGG	GTGCTCCTGGTTCTGTTCTT	CTCGGGTGTCTTGTCACTTT	1
Glut2	GAACTGCCCACAATTGCATAC	GGGACCAGAGCATAGTGATTAG	ATCCTTCAGTCTCTGCTACTCT	GCTTTGCTTTGACTTCCTCATC	1
Glut3	AGGATGCAGGTGTTGAAGAG	GCCCTTTCCACCAGAAATAGA	CCTCTGCTGCTCACTATTTAGG	GGTCTCAGGGACTTTGAAGAAG	1
Glut4	GGCTTCTTCATCTTCACCTTCT	GGTTTCACCTCCTGCTCTAAA	CCTCTGCTGCTCACTATTTAGG	GGTCTCAGGGACTTTGAAGAAG	2
Glut5	GGCTTCTTCATCTTCACCTTCT	GGTTTCACCTCCTGCTCTAAA	GCCCTACGTCTTCCTTCTATTT	AGCTGAGATCTGGTCAAACG	2
Glut6	CCAAAGAGAGAGGTGGAACTG	ACGTCACCCAGGTAGTAAGA	CTTTGGGTATGCTCTGGTCTAC	ATGCCTGGGATTTGGTCAG	2
Glut7	CATCGGTGCCTACAGTTTCA	GCCCTTGGTCTCAGGAATAAC	ACTGGCTCACCAACTTCATC	GAGGCAGATTCCGGCAAATA	1
Glut8	GGCATCTACAAGCCCTTCAT	GTCCTTGAACTTGGCCTCTT	CCAAGACGTGTGGATGCT	GGTAGGCGATTTCAGAGATGTAG	1
Glut9	CAGGTGAAGTTGCCATGATCTA	CCCTCCCAGAACACCTTATTTC	CTGCCATCTTTATCTGCATTGG	TCGGGAAACATCTGCCTTAC	1
Glut10	GATCTACCCTGTGGAGATACGA	GGAGAGGCTGATGAAGAGATTG	ATAGGAGGCTTCAGCTCTAGT	CTTGTCCAGGCTTCCCATTAT	1
Glut11	CTGCGGGAATGACTTGATGTA	GATGGTGGCATACTGGACTTT	GTTGGCAGCGATTCTGTTTG	CAGGTACATGGGCTGGATATT	1
Glut12	GACCTCAGCATCCTTGCTAAA	TGGCTAAGGACAGCCATTTC	CATGAGCAGGAAATGGTTGTG	TTGCGGTCCTTCTTCCATAC	1
Glut13	GGTACCACTGTAGCACTCATTAT	GTTCTGACCTGACGGAGTTATT	CCAGCAACTCTCAGGCATTA	CTGTAACTGAAGCCAGCCATA	1
Glut 14	CCTCCGCTGCTTACTATTTAGG	GTCTCAGGGACTTTGAAGAAGG	CCAAGACATCCAGGAGATGAAA	TCGGTAGCTGGACACTCTAA	1

All primer sets were tested by RT-PCR and gel electrophoresis. (Figure 2) The primer set showed higher performance were selected for future use based on their band

clarity, intensity, and the presence of additional bands. Selected primer sets were listed on Table 7.

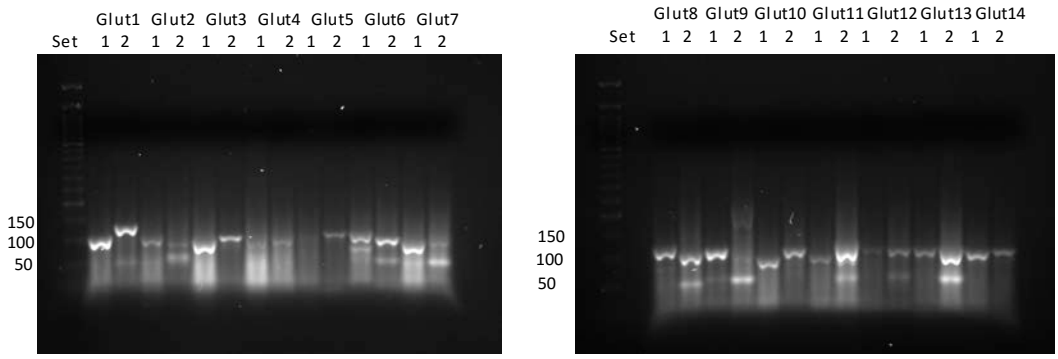

Figure 2 Primer test resuts on agarose gel

Two sets of primers were tested by RT-PCR. Left: Glut1-7. Right: Glut8-14

4.1.2 Confirm glucose transporter expression on a gel

Granulomas are highly variable in their avidity for FDG and we do not know how variable Glut expression is between monkeys or granulomas, and so we tested our primers by RT-PCR on RNA from a pool of granulomas from multiple monkeys to improve our chances of selecting primers and minimize our chances for false negatives. DNA products were visualized by 2% agarose gel electrophoresis (Figure 3), demonstrating all product sizes were around 100 bp, which were consistent with their predicted amplicon lengths. On the left, Glut1 and Glut 3 had relatively stronger expression than the others. Glut4, 5 and 6 were weaker and Glut2 and 7 showed to be the weakest. On the right, except Glut8 and 14 show relatively high expression, the rest have either very low or no expression.

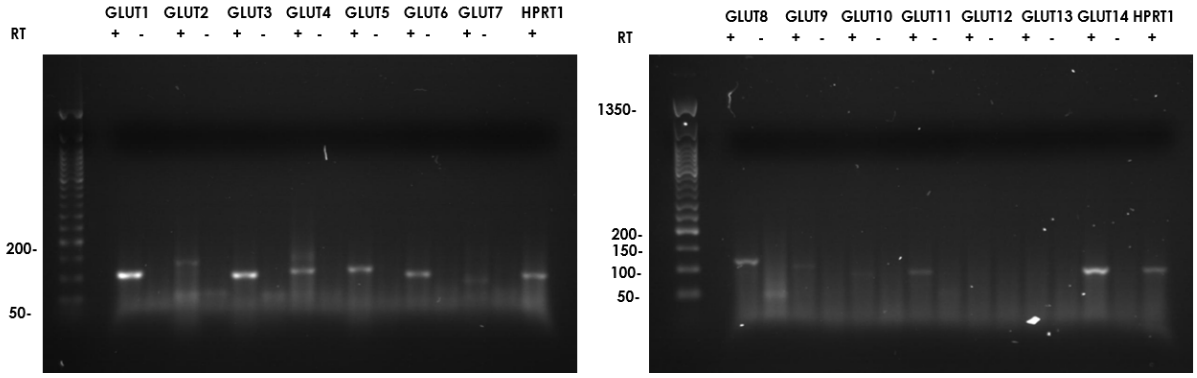

Figure 3 Glucose transporter expressions by RT-PCR

Expression of glucose transporter 1-14 and their no RT control next to them. First lane: DNA ladder. Lane 2-15: expression of glucose transporter. Lane 16: Expression of HPRT2 reference gene.

4.1.3 Quantification of Glucose transporter expression by qRT-PCR

To further examine the glucose transporter expression and examine the diversity of expression across multiple granulomas, we isolated RNA from 9 pieces of cryopreserved normal lung and 10 cryopreserved granuloma-containing pieces of lung tissue with known SUV levels (Figure 4). The RNA was transcribed into cDNA and qPCR was performed to measure the glucose transporter mRNA expression. The result were presented as fold change glucose transporter expressions relative to HPRT1 expression (Figure 5) calculated with delta CT values and $2^{\wedge(-\text{delta CT})}$.

We found that, except Glut3, the rest of the glucose transporters had lower expression relatively to HPRT1 expression in granulomas than uninvolved normal tissues (Figure 6A-C). Glut3 was expressed at a higher level (lower Ct) than HPRT1. Expression of some glucose transporters in granuloma tissues were much lower than normal tissue which was opposite of our expected results. For instance, expression of Glut1, 2, 7 and

13 in granulomas was at least 5-fold lower than the expression in normal tissues. Others including Glut4, 6 and 11 also showed lower expression in granulomas than in normal tissue, whereas Glut3, 5, 8 and 14 had similar expression patterns in normal lung and granulomas (Figure 5A-5C). Despite some tissues that have high SUV values (red markers) there was considerable variation in Glut expression (Figure 5A-5C). This distribution suggest that glucose transporter expression is not directly related to FDG uptake and PET-CT measured SUV. Glut3 was the only glucose transporter showing higher expression relative to HPRT1 and was also expressed at significantly higher levels than Glut1, 2, 11 and 13. Besides Glut4 5, 6, 8 and 14 were their expression was moderately close to their HPRT1 expression, the other Gluts had much lower expressions relative to HPRT1 (Figure 5D).

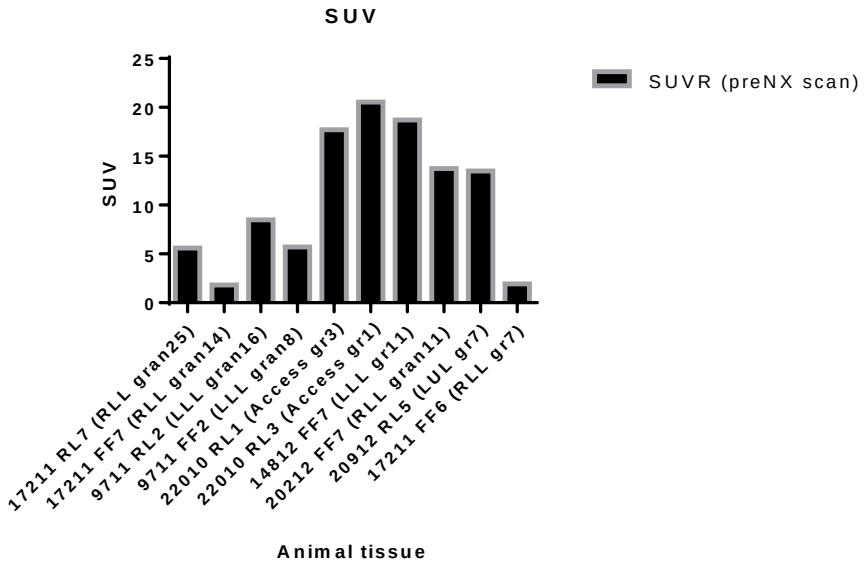

Figure 4 SUVs of the 9 ranulomas used in this study

Granulomas with known SUV, with 5 low SUV tissues on the left and 5 high SUV tissues on the right and name of the tissues at bottom.

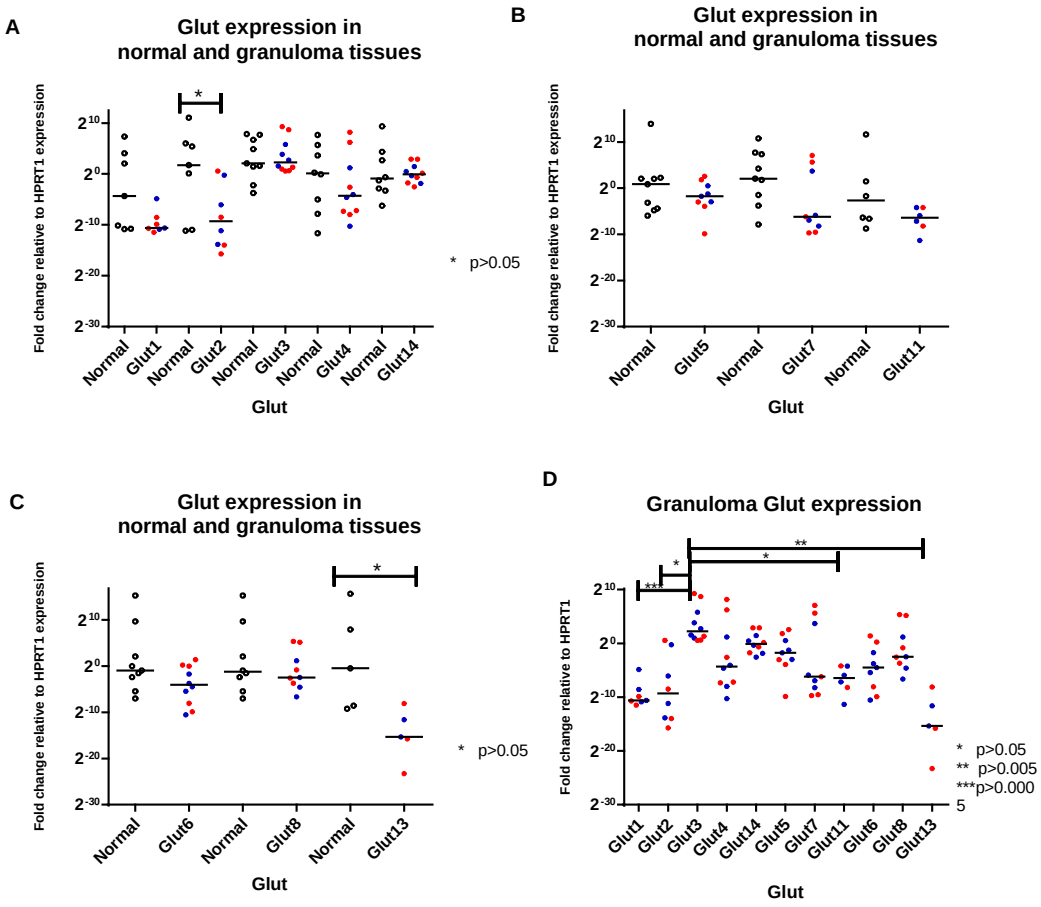

Figure 5 Glucose transporter expression relative to HPRT1

(A). Class I glucose transporter expression in normal tissues and granulomas.
(B). Class II glucose transporter expression in normal tissues and granulomas.
(C). Class III glucose transporter expression in normal tissues and granulomas.
(D). All Glucose transporter expression in granulomas.
Glucose transporter expression in normal tissues are shown in hollow points, tissues with high SUV level are shown in red, tissues with low SUV levels are shown in blue. Dash line represents median level. Asterisk represents significant differences between two groups.

Then, we performed a correlation analysis to determine if expression of any of the glucose transporters were correlated with granuloma SUV levels. None of our analyses demonstrated clear relationships or statistically-significant correlations between SUV and Glut expression (Figure 6A-K). Altogether, based on our small sample subset, the results

suggest there is not a clear link between individual glucose transporter expression and higher SUV levels in nonhuman primates.

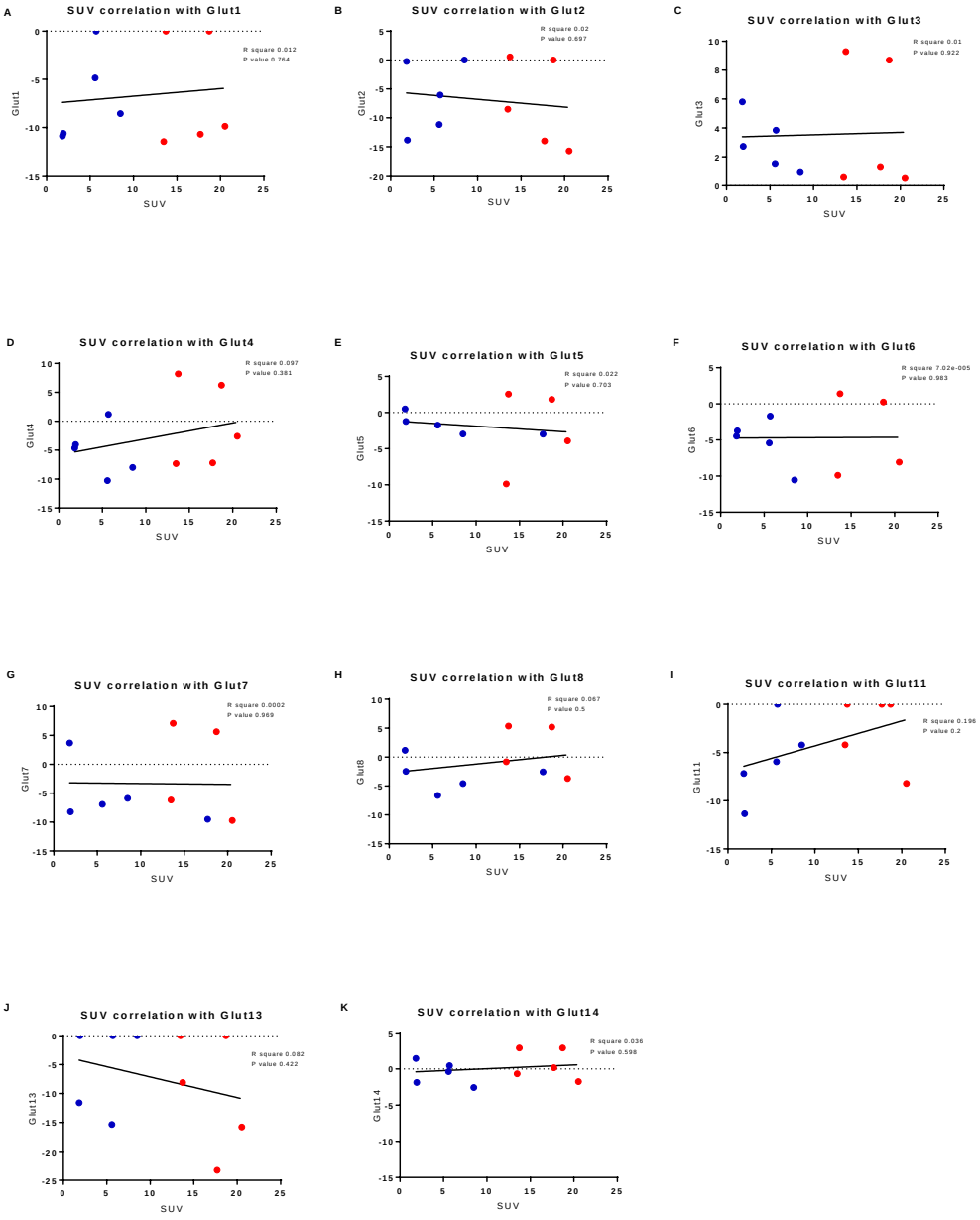

Figure 6. SUV level correlation with glucose transporter expressions

(A-K). Glucose transporter 1-14 expression and their correlation with SUV. Animal tissues from low SUV group shown as blue and high SUV group shown as red. R2 and P value were shown on the right. Dash line represents no expression.

4.2 AIM 2: IDENTIFY CELLS EXPRESSING GLUCOSE TRANSPORTERS AND THEIR PATTERN OF LOCALIZATION IN GRANULOMAS

4.2.1 Fluorescent immunohistochemistry on granulomas

Although our RT-PCR data did not demonstrate a relationship between individual Glut mRNA expression and SUV, we next tried to correlate Glut protein expression with SUV and localize expression in granulomas. To identify where glucose transporters might be expressed in granulomas and determine which cells are associated with glucose transporter expression, we performed fluorescent immunohistochemistry on two representative necrotic granulomas from different monkeys for Glut1, 2, and 3 (Figure 7). Glut1 staining was strong and Glut1-positive cells were most abundant near the necrotic center where macrophages and neutrophils were rich. Glut2 expressions was significantly weaker and scattered around the outer region of the granuloma and in the uninvolved lung. Glut3 had a similar expression pattern to Glut1 and was also expressed in the tissue adjacent to the granuloma in the first monkey. HIF1-α, a protein expressed under hypoxic conditions was restricted to the inner region of the two granuloma, confirming the hypoxic nature of these granulomas. Calprotectin-stained neutrophils were mostly concentrated in the center of the two granuloma but were also found scatter around the tissues. CD3+ T cells and CD20+ B cells were shown to be mostly present in the lymphocyte cuff. As for macrophage populations, CD11c+CD206- negative epithelioid macrophages were located near the center of the two granulomas, while CD11c-CD206+ alveolar macrophages were only seen at the granuloma's outer rim. In summary, these results

suggest Glut1 and 3 are strongly expressed in the region occupied by epithelioid macrophages and neutrophils.

A

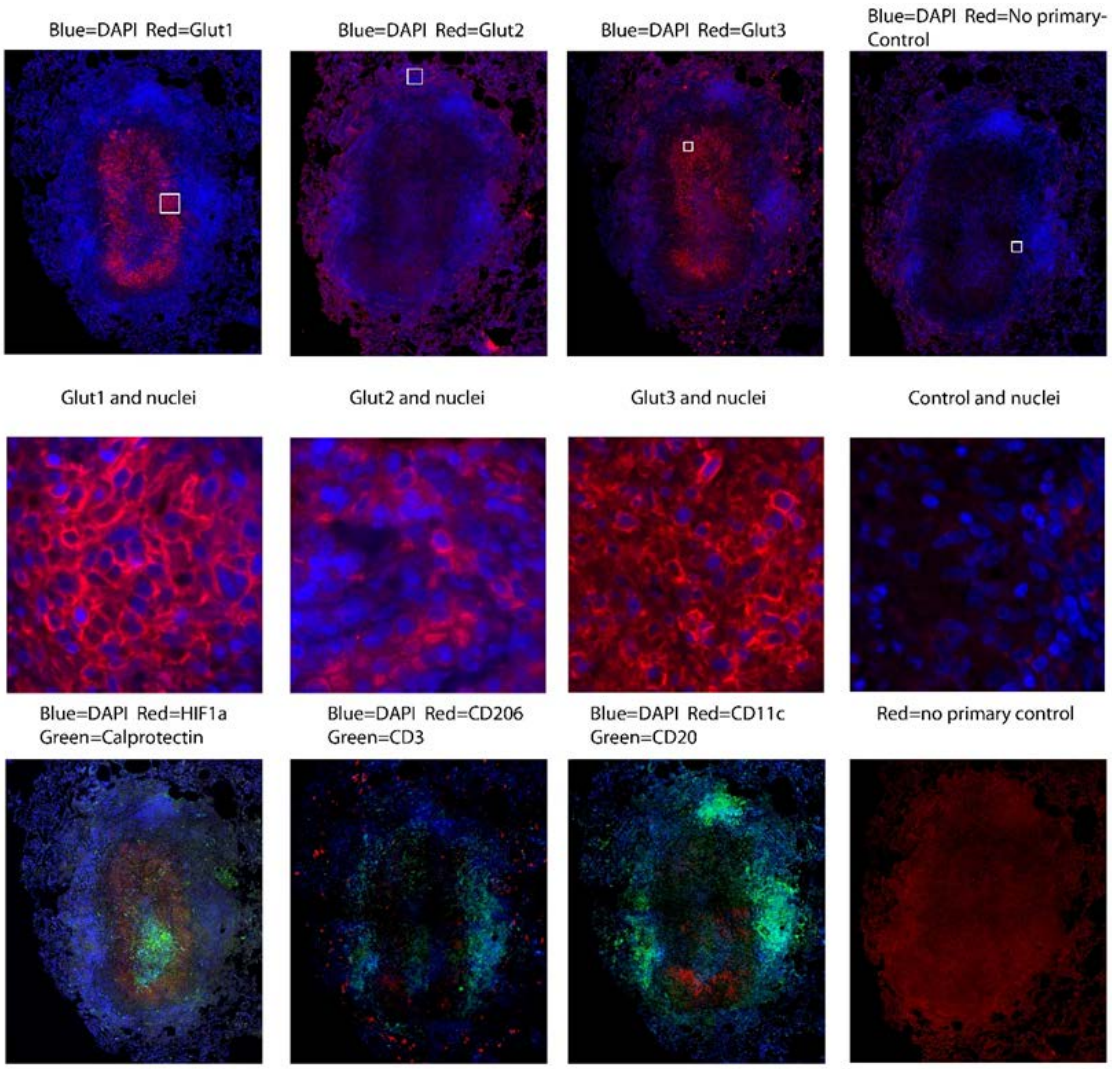

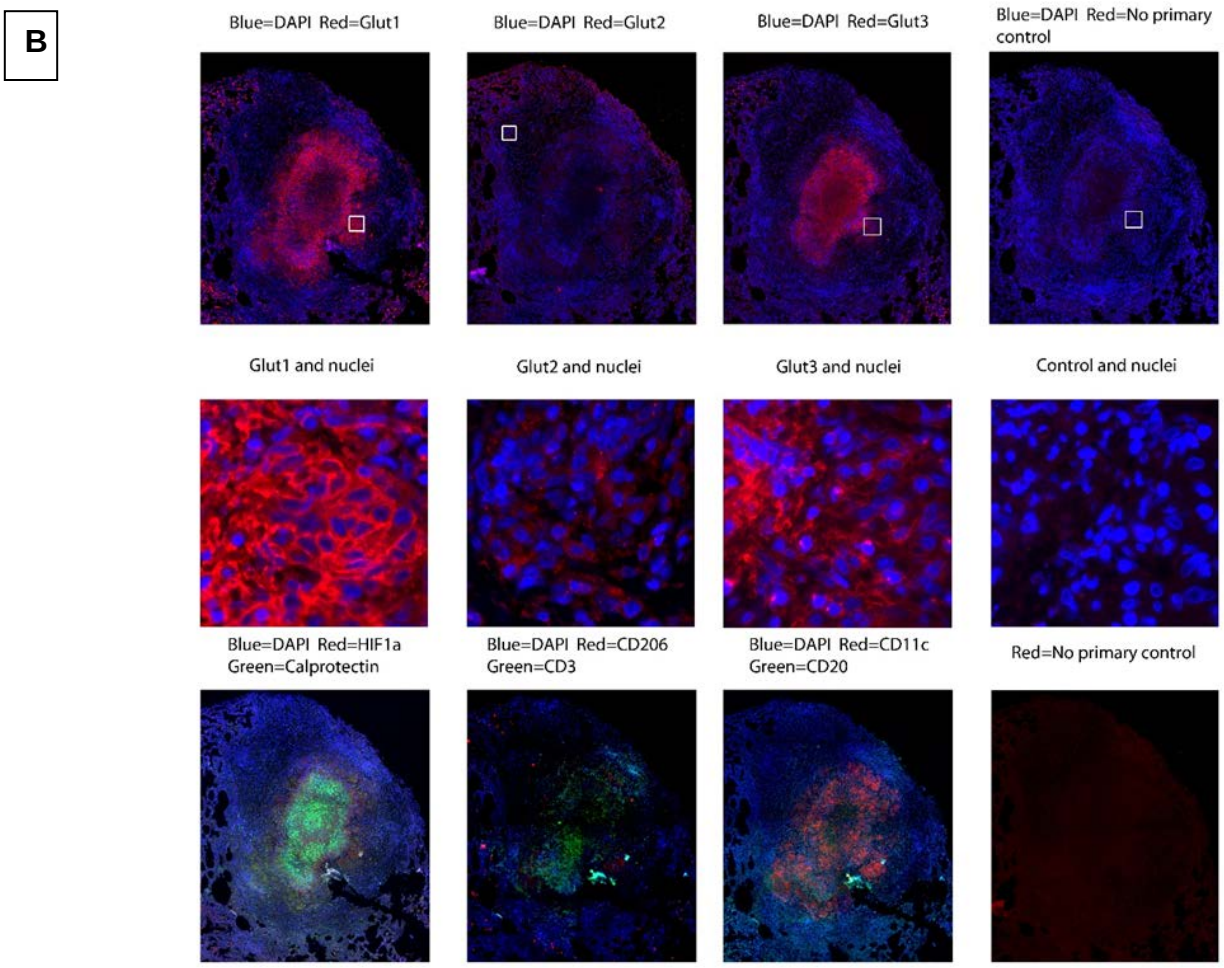

Figure 7 Localization of glucose transporter and cell populations from IHC

(**A** and **B**). First line: Expression of glucose transporter 1, 2 and 3 (red), nuclei (blue) and no-primary control. Second line: High magnification of glucose transporter expression from the white box. Third line: Hypoxic cells were stained with HIF1-a (red), Calprotectin stained neutrophils (green) and lymphocytes were stained with CD3 (green), CD20 (green). Macrophage-specific antibodies stained CD11c (red) for both epithelioid and alveolar macrophages, but CD206 (red) for alveolar macrophages only. Nuclei were shown in blue.

4.2.2 Mean Fluorescent Intensity and correlation with SUV

Our RT-PCR experiments examined mRNA expression, but to better understand glucose transporter protein expression, we performed immunohistochemistry on granulomas with high or low SUV levels. We analyzed the fluorescence as a metric for

protein expression and compared the high and low groups for glucose transporter expression. We were limited to glucose transporters with antibodies that work in formalin-fixed paraffin-embedded tissue sections, and so we examined Glut1-4 expression. We used 11 tissues in this study; 6 had high SUV levels and 5 had low SUV levels (Figure 8). Glucose transporter expression was measured as Mean Fluorescent Intensity in granulomas defined by regions of interest and quantified with Nikon Elements. We first counted the cell numbers in the regions of interest to see if there was a trend of higher cell numbers (indicative of more inflammation) in tissues with high SUV levels (Figure 9). Tissues used for Glut1 and 4 staining had slight higher numbers of cells/ROI in the High SUV tissue group than low SUV tissue group but the difference was not significantly different between groups. Glut2 had very similar cells/ROI in the two groups and Glut3 had slight lower cell/ROI in the high SUV group than low SUV group. None of the group shown to have number of cells significantly different from each other in terms of cell number/region of interest suggesting that differences in SUV/granuloma are not associated with total numbers of cells per granuloma.

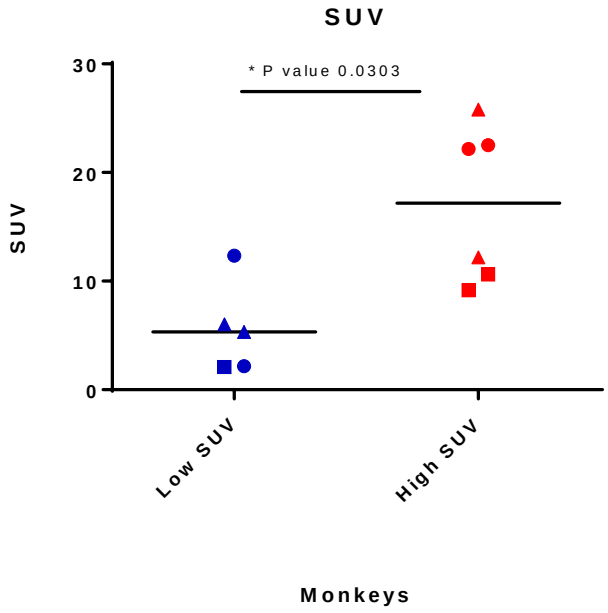

Figure 8 SUV level from granuloma tissues

Granuloma tissues were separately in low SUV group shown in blue or high SUV group shown in red. Asterisk indicates a significant difference between the two groups ($p<0.025$).

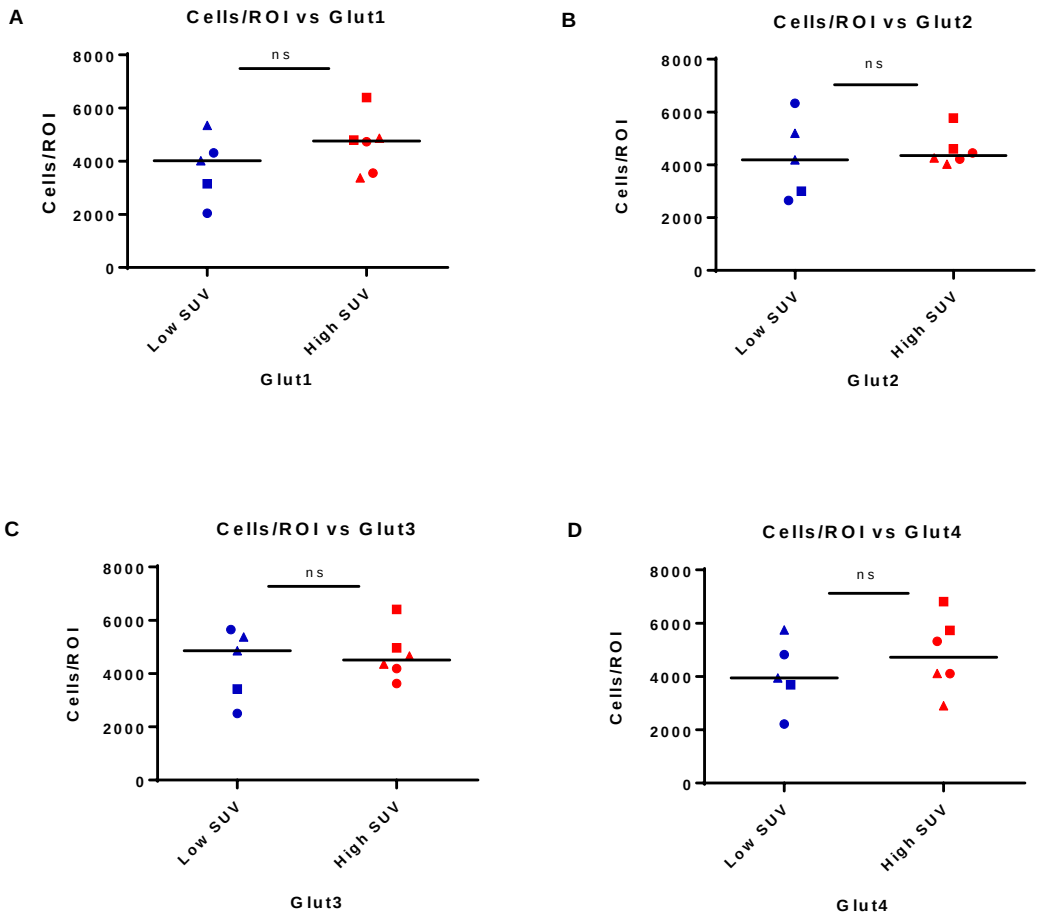

Figure 9 Glucose transporter expression measured by Cells/ROI in low and high SUV group

(A-D). Individual glucose transporter expression comparison between low and high SUV groups. Low SUV group shown as blue and high SUV group shown as red. Dash line represents median level of the expression. Not significant difference between the groups shown as ns.

Next, we looked at the mean fluorescent intensity (MFI) of each glucose transporter (Figure 10A). We did not do statistical comparisons on glucose transporters because each antibody has its own level of background and avidity, but overall median MFI for glucose transporters were not substantially different from each other (Figures 10A-E) in terms of overall expression (Figure 10A) or comparisons between low and high SUV groups (Figures 10B-E). Correlation analysis showed weak positive correlation

between their Glut MFI and SUV levels (Figure 11A-D), suggesting that expression of the glucose transporter we are examining here are poorly correlated with granuloma FDG uptake.

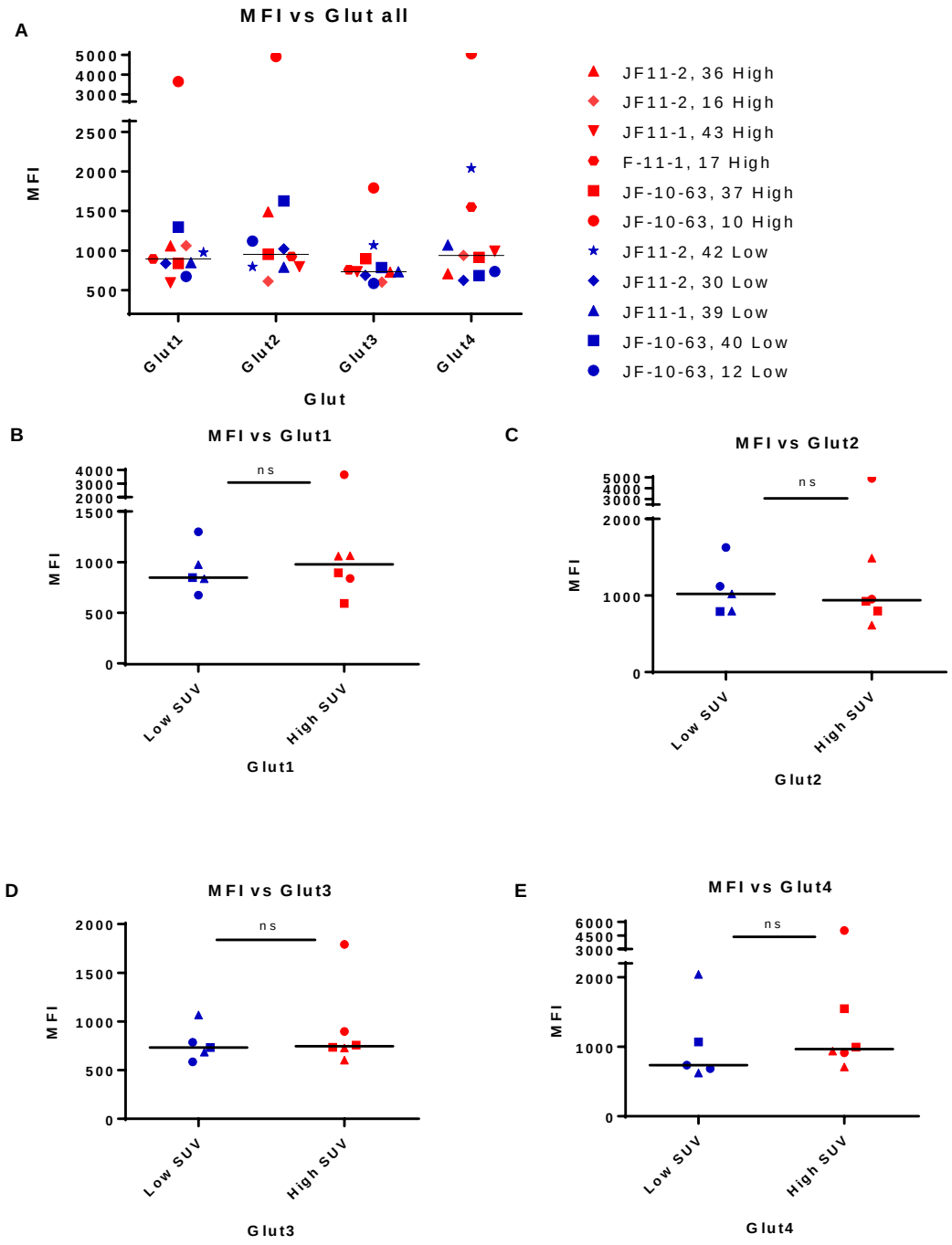

Figure 10 Glucose transporter expression measured by MFI in low and high SUV group

(A). Glucose transporter expression from different animal tissues manifest as MFI. Animals with low SUV are shown in blue and high SUV animals are shown in red with the median expression indicated. Animal tissue numbers are shown on the right.
(B-E). Individual glucose transporter expression comparison in MFI between low and high SUV groups. Low SUV group shown as blue and high SUV group shown as red. Dash line represents median level of

the expression. Not significant difference between the groups shown as ns.

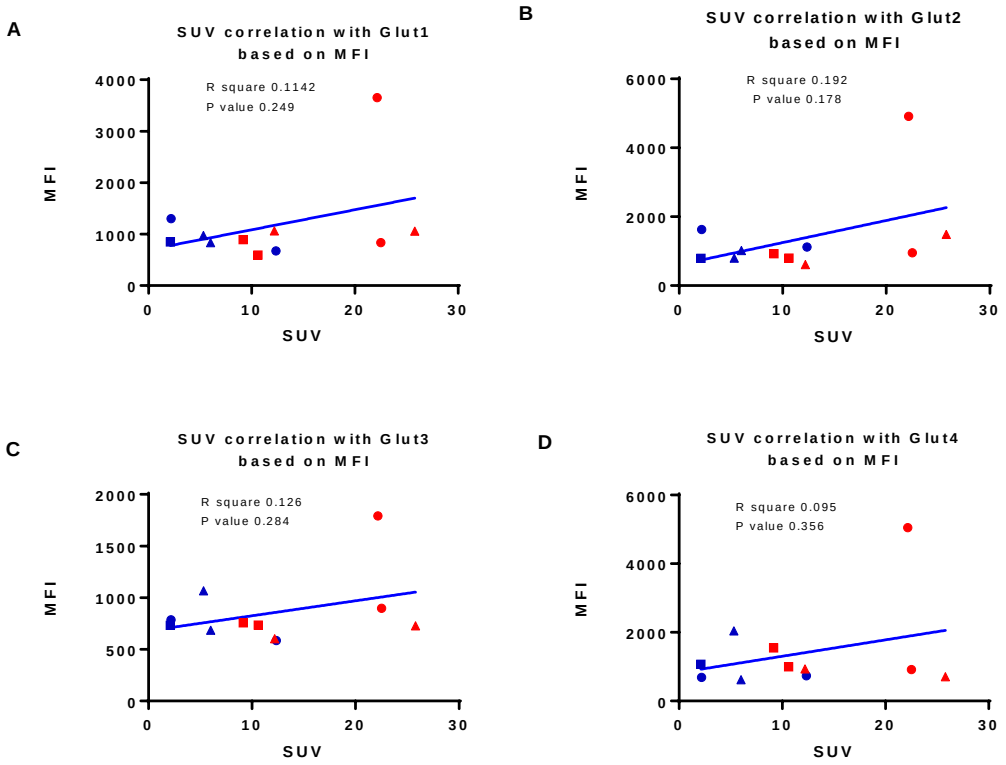

Figure 11 SUV correlation with glucose transporter expression based on MFI levels

(A-D). Expression of glucose transporter 1-4 measured by MFI and their correlation with SUV. Animal tissues from low SUV group shown as blue and high SUV group shown as red. R2 and P value are indicated in the graphs.

We next calculated MFI/ROI (mm2) for each glucose transporter expression to determine how glucose transporter expression related to granulomas when normalized for size (Figure 12). This analysis was highly similar to the MFI data without normalization and we did not observe significant differences between the SUV high or low groups (Figure 12A-E), or correlation between MFI/Area and SUV (Figure 13A-D). These data suggest that our lack of correlation is independent of the size of the granulomas we examined in this study.

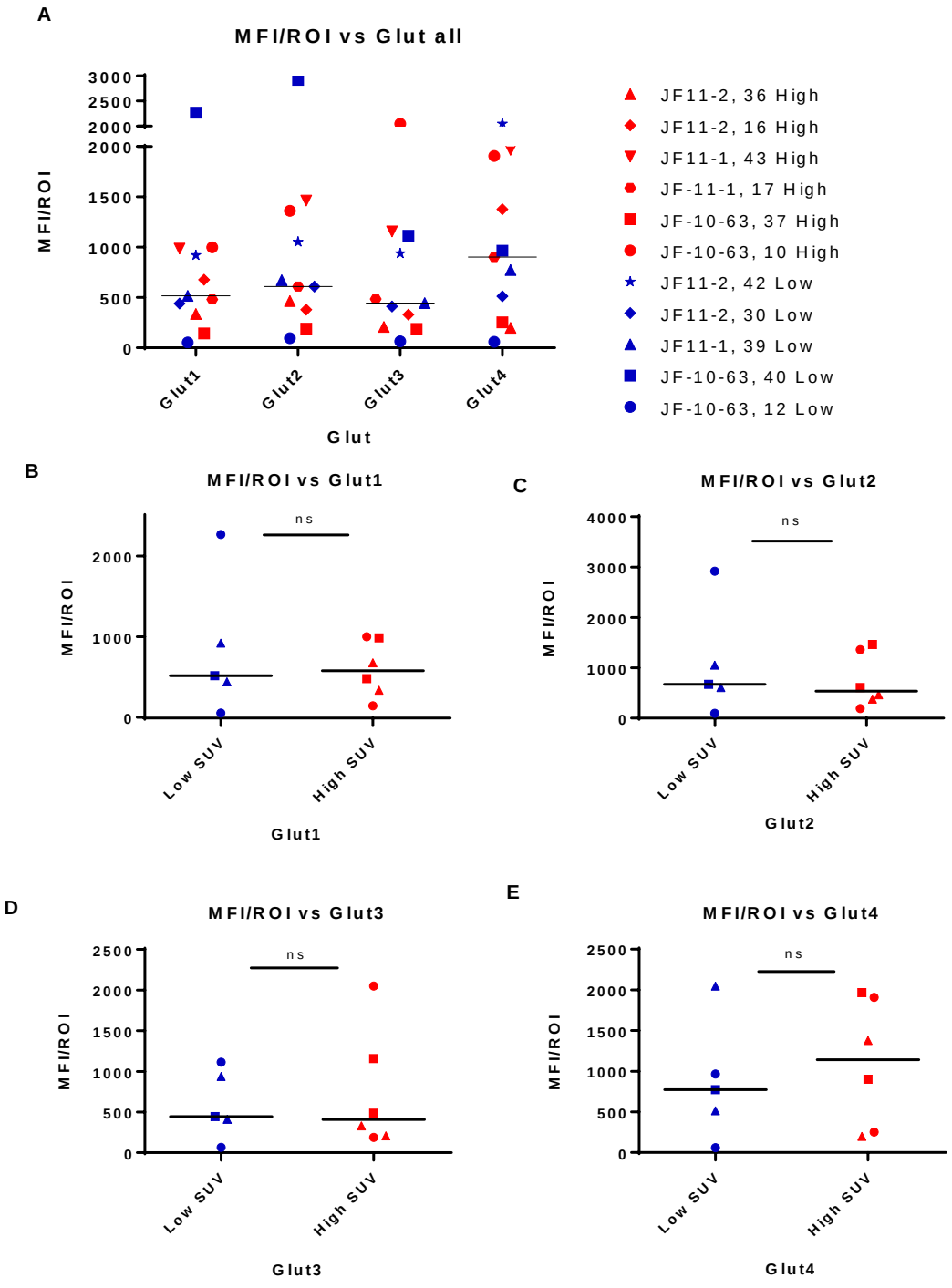

Figure 12 Glucose transporter expression measured by MFI/ROI

(A). Glucose transporter expression from different animals was calculated as MFI/ROI to normalize for different-sized granulomas. Low SUV granulomas are shown in blue and high SUV granulomas in red with the median. Animal and tissue numbers are shown on the right.

(B-E). Individual glucose transporter expression comparison for MFI/ROI between low and high SUV groups. The low SUV group is shown as blue and high SUV group is shown as red with the median. Non-significant differences between the groups are indicated as ns.

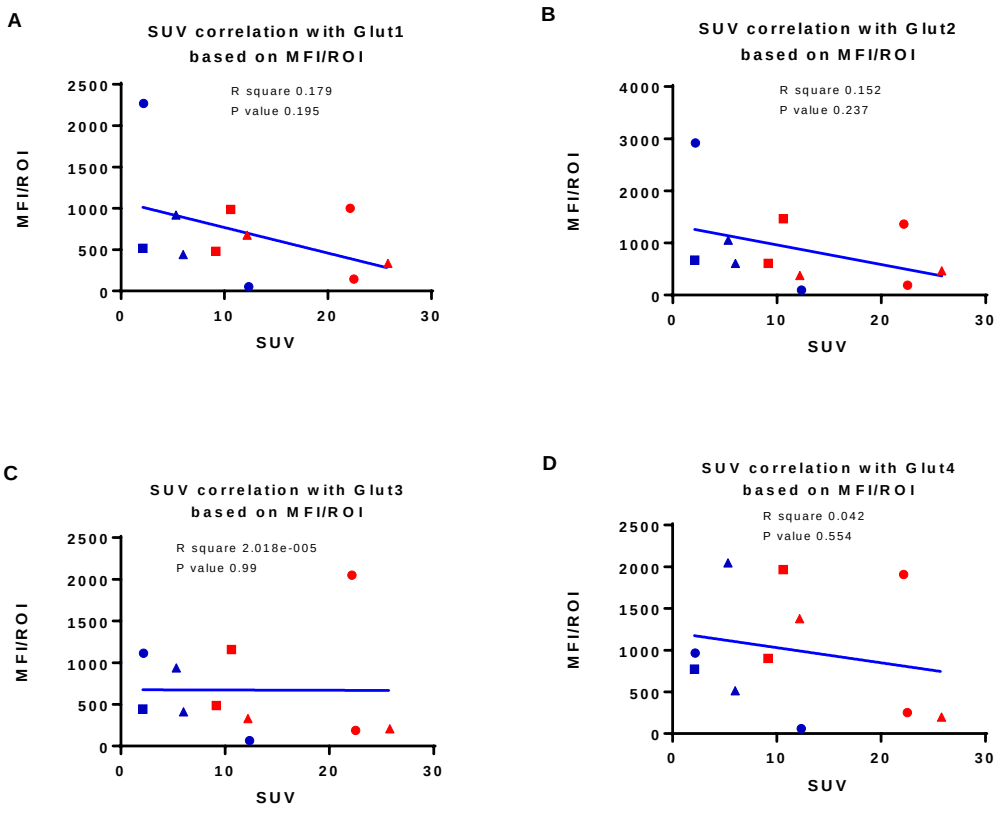

Figure 13 SUV correlation with glucose transporter expression based on MFI/ROI levels

(A-D). Expression of glucose transporter 1-4 measured by MFI/ROI and their correlation with SUV. Animal tissues from low SUV group shown as blue and high SUV group shown as red. R2 and P value are indicated in the graphs.

Next, we measured MFI/Nucleus to determine the relationship between cell numbers and overall glut expression (Figure 14). As with previous analyses, there were variations between granulomas within each glucose transporter (Figure 14A), however we did not identify significant differences between cells per granuloma and glucose transporter signal (Figure 14 B-E). Similarly, we did not identify a correlative relationship

between SUV and MFI/nucleus (Figure 15A-D) suggesting that glucose transporter expression was independent of the total number of cells per granulomas.

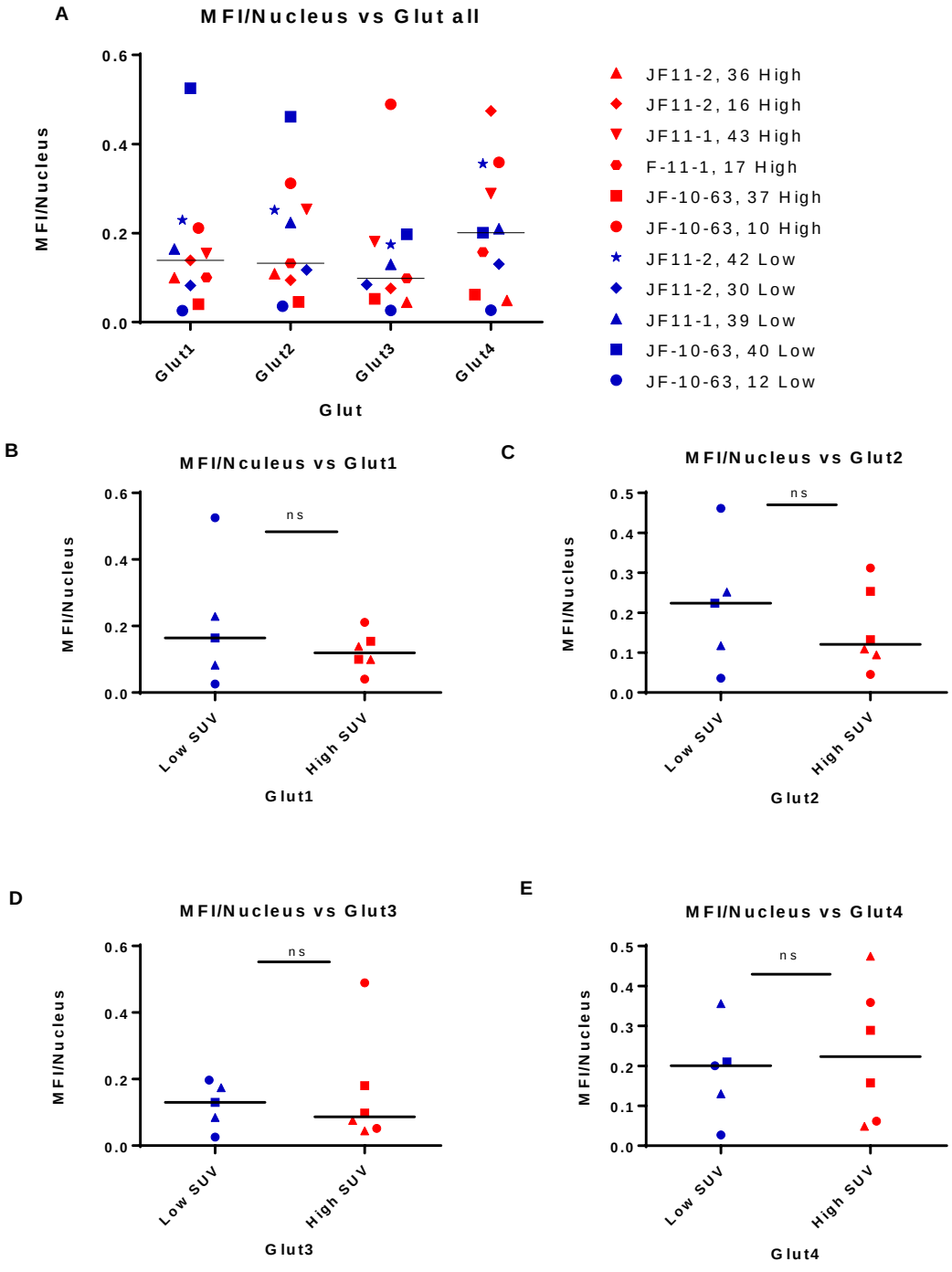

Figure 14 Glucose transporter expression measured by MFI/Nucleus

(A). Glucose transporter expression from different granulomas presented as MFI/Nucleus. Low SUV granulomas are shown in blue and high SUV are shown in red with lines indicating medians. Animal and tissue numbers are shown on the right.
(B-E). Comparison of glucose transporter MFI/Nucleus between low and high SUV groups. The low SUV group shown as blue and high SUV group shown as red with dashed lines indicating medians. Non-significant differences between the groups are indicated as ns.

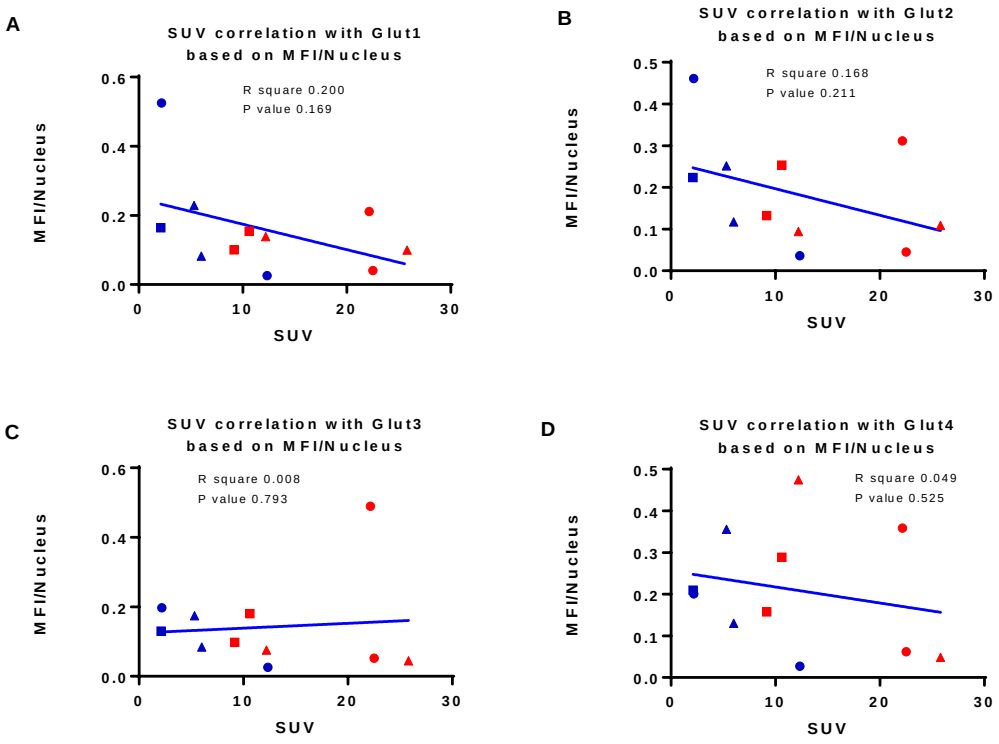

Figure 15 Correlation of SUV and glucose transporter MFI/Nucleus

(A-D). Gluts1-4 MFI/Nucleus and their correlation with SUV. Low SUV group granulomas are indicated in blue and high SUV group in red. R^2 and P value are indicated in the graphs.

These data suggest that gluts1-4 are not strongly correlated SUV when glucose transporter expression is measured in terms of MFI, MFI/area, or MFI/nuclei (a measurement of a granuloma's inflammatory state). To further refine our analysis, we sought to compare the cell types within a granuloma with glucose transporter expression. We found our staining for macrophages and T cells was not sufficient for quantitative analyses of these cell types, and B cells were present in tight clusters that could not be

segmented into separate cells (Figure 7). Neutrophils were the most easily counted cell type in our images, and to determine if neutrophils are correlated with SUV levels, we counted their numbers with Nikon Elements and correlated neutrophil numbers with the granuloma's SUV (Figure 16 A-B). There were more neutrophils in the high SUV group than low SUV group and the number of neutrophils present in the granuloma was strongly correlated with SUV levels which suggests higher neutrophils numbers are associated with higher SUVs in granulomas.

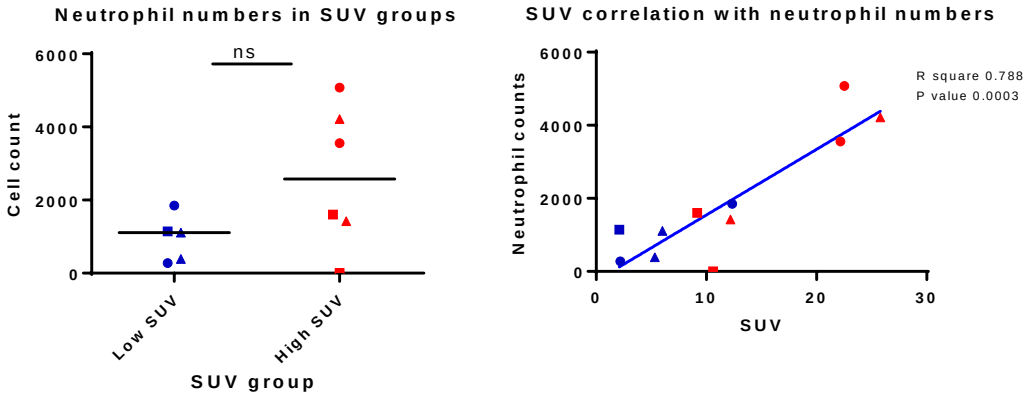

Figure 16 Neutrophil SUV correlation with neutrophil numbers

(A). Comparison of neutrophil numbers between low and high SUV groups. **(B).** Neutrophils numbers were plotted against SUV/granuloma. Low SUV granulomas are indicated in blue and high SUV granulomas in red.

5.0 DISCUSSION

Despite the enormous effort spent fighting against TB, this disease still poses a major threat to global health and surpassed HIV to become the leading cause of death from infectious disease in 2015 (61, 62). Delayed detection is a problem in diagnosing TB but PET/CT imaging technology offers a powerful tool of detecting active TB in a fast and efficient manner. Currently, most PET/CT imaging uses a glucose analog (FDG) to identify inflammation. However, inflammation in granulomas is an extreme complex process and the mechanism of inflammation, and metabolic changes associated with FDG uptake remains to be elucidated. We hypothesize that there are links between inflammation states in granulomas that can be associated with glucose transporter expression and inflammatory cell types. In our studies, we sought to characterize glucose transporter expression during FDG PET/CT-measured inflammation and identify the cell types responsible for FDG uptake.

Our initial RT-PCR results on pooled RNA from multiple granulomas indicates expression of some glucose transporters, including Glut1 and Glut3, is higher than others. Upregulation of Glut1 and Glut3 have been previously reported in a study using the murine TB model (36) and high level of Glut1 and 3 have also been found in activated macrophages and lymphocytes (63) and our results appeared to confirm this in nonhuman primates. However, the results we obtained with qRT-PCR on RNA from individual granulomas with known SUVs were somewhat different. All glucose transporters except Glut3 had lower expression relatively to HPRT1 and there was considerable variation of Glut expression in normal tissues and granulomas. Correlation

analysis based on delta Ct values also didn't indicate any significant positive relationship between glucose transporter expression and higher SUV levels. These data suggest that FDG uptake in granulomas is complex and cannot be explained by comparing individual glucose transporter expression with SUV. Using a more sophisticated statistical technique, such as Principle Component Analysis, that accounts for multiple factors in the analysis may help clarify this.

We performed IHC on granulomas to localize glucose transporters in granulomas and to identify the cells that contribute to Glut expression. Initially, we identified strong expression of Glut1 and Glut3 in the rim of cells that surround the granuloma's necrotic center, a region where epithelioid macrophages and neutrophils are abundant. The staining pattern indicated the strongest expression occurs on epithelioid macrophages, but some neutrophils also appeared to stain positively. We also observed strong HIF1α expression in this region. HIF1α's expression is closely associated with induction of the Warburg effect and has been identified in the immune activation and responses to infection (11, 45-47) and future studies will determine if increased HIF1α expression and upregulation of glucose transporter expression occur during proliferation of epithelioid macrophages in granulomas. In contrast to epithelioid macrophages, lymphocyte-rich areas were not strongly Glut1 or Glut3 positive suggesting these cells are not major contributors to expression of these glucose transporters. That said, we cannot rule out the possibility that lymphocytes express high levels of other Gluts we could not examine by IHC, or interactions between lymphocytes and epithelioid macrophages play roles in inflammation and increases in granuloma FDG uptake. Glut2 had much lower expression in this region and, consistent with previous finding (64), and it was mostly seen on

epithelial surfaces. Then we used tissues with known SUVs to further characterize the relationship between expression of glucose transporters and FDG uptake. This time, the staining pattern showed the greatest expression of Glut4 in granulomas compared to the rest of the glucose transporters, although no significant differences were found between the groups. We examined both total cell numbers and MFI-related measurement to determine whether there were SUV-related differences in Glut expression, but found no significant differences or strong correlations between high and low SUV in any of the group. These data further suggest that no single Glut is responsible for FDG uptake. Alternatively, other factors may contribute to this lack of variation. Firstly, the tissues sections of the granulomas used for this study were small, were sometimes incomplete (lacking easily distinguished epithelioid macrophage populations), and had cutting-related artifacts (folds) that were difficult to compensate for. Variations in the type of granuloma (necrotic or non-necrotic) and our small sample size (5 granulomas for the low SUV group and 6 in the high SUV group) may also have contributed.

So, taken together, initial RT-PCR and IHC results support elevated expression of Glut1 and Glut3 in granulomas but further characterization from the two systems with known SUV groups show large variation and discrepancy that could not be correlated with elevated SUV. There were also some inconsistencies between the RT-PCR and IHC results, including variation in Glut1 expression. It's hard to determine the exact cause of these differences but we believe variables including small sample size, antibody affinity in IHC, background in images, variability in tissue quality influenced the IHC results, while qRT-PCR was affected by our choice of housekeeping gene and amplification efficiencies. On the other hand, neither of the two systems indicate any significant

correlation between individual glucose transporter expression and their SUV levels, which suggest either glucose transporters are not driving FDG uptake or that the system is more complex than we thought and current method we use for analysis might not be sufficient for this study. Furthermore, a correlation was found between neutrophil numbers and SUV. Large numbers of neutrophils are associated with poorly controlled disease (65-67) and these data suggest neutrophil numbers least partially contribute to FDG uptake and higher SUV in granulomas. However, no relationship was found between MFI/Nucleus and SUV suggesting in a complex structure like a granuloma where large numbers of cells are clustered together that cannot be differentiated as easily as neutrophils, a small population of cells might have a large contribution to SUV and our analysis might not be sensitive enough to measure this difference. Our evidence that epithelioid macrophages, a population we were not able to reliably count, express large amounts of Glut1 and Glut 3 support this. A different approach, possibly focused on particular regions in granulomas (e.g. lymphocyte cuff vs epithelioid macrophages) with more detailed analysis of different cell types will be needed to confirm this.

We believe our study may provide new insight and perspective of studying metabolic and physiological characteristics in granuloma. With better comprehension of glucose transporter expression profile in the granuloma, it may not only enhance our overall understanding of the complex and dynamic changes within granulomas, but may also open a new route of testing potential glucose tracers that may improve the sensitivity and usefulness of existing PET/CT imaging technology.

6.0 FUTURE DIRECTION

Our study provided preliminary data for glucose transporter expression patterns in primate granulomas, but many questions remain unanswered, for instance, we believe epithelioid macrophages might play prominent roles in driving FDG uptake but we were unable to quantify their numbers and glucose transporter expression associate with them. Future experiment should focus on using approaches analyzing glucose transporter expression on epithelioid macrophages and other cell types in addition to neutrophils. Also, a more powerful analytic strategy such as Principle Component Analysis (PCA), which can identify correlations between multiple factors and determine the factors best explaining variation in a system, could be used more fully explore this data. We would use PCA to examine the relationship between different glucose transporters, cell types, and numbers of cells to more fully explore how glucose transporter relate to FDG uptake. Lastly, metabolic change and immune responses in granulomas are complex and related (11, 36, 44, 68). The earliest granulomas that can be identified by PET/CT occur at about 3 week post infection, and this is approximately the time when anti-Mtb adaptive immune responses develop. This suggests that development of hypoxia and the Warburg effect may be related events where adaptive immune cells induce differentiation of epithelioid macrophages and upregulated glucose transporter expression, and eventually change the microenvironment of the granuloma. Future experiments should also include granulomas from early post-infection necropsies to determine how glucose transporter expression changes in early and late granulomas. By studying glucose transporter

expression we may improve our understanding of the other events taking place in granulomas and apply these findings to ways that benefit to TB treatment.

BIBLIOGRAPHY

1. **Delogu G, Sali M, Fadda G.** 2013. The biology of mycobacterium tuberculosis infection. Mediterr J Hematol Infect Dis **5:**e2013070.
2. **Organization WH.** 2016. Global tuberculosis report 2016.
3. **Sathekge M, Maes A, Van de Wiele C.** 2013. FDG-PET imaging in HIV infection and tuberculosis. Semin Nucl Med **43:**349-366.
4. **Corbett EL, Bandason T, Cheung YB, Munyati S, Godfrey-Faussett P, Hayes R, Churchyard G, Butterworth A, Mason P.** 2007. Epidemiology of tuberculosis in a high HIV prevalence population provided with enhanced diagnosis of symptomatic disease. PLoS Med **4:**e22.
5. **Organization WH.** 2017. Tuberculosis Fact Sheet.
6. **Russell DG, Barry CE, 3rd, Flynn JL.** 2010. Tuberculosis: what we don't know can, and does, hurt us. Science **328:**852-856.
7. **Brewer TF.** 2000. Preventing tuberculosis with bacillus Calmette-Guerin vaccine: a meta-analysis of the literature. Clin Infect Dis **31 Suppl 3:**S64-67.
8. **Colditz GA, Brewer TF, Berkey CS, Wilson ME, Burdick E, Fineberg HV, Mosteller F.** 1994. Efficacy of BCG vaccine in the prevention of tuberculosis. Meta-analysis of the published literature. JAMA **271:**698-702.
9. **Ritz N, Hanekom WA, Robins-Browne R, Britton WJ, Curtis N.** 2008. Influence of BCG vaccine strain on the immune response and protection against tuberculosis. FEMS Microbiol Rev **32:**821-841.
10. **Organization WH.** 2015. Immunization, Vaccines and Biologicals-Tuberculosis vaccine development http://www.who.int/immunization/research/development/tuberculosis/en/.
11. **Shi L, Eugenin EA, Subbian S.** 2016. Immunometabolism in Tuberculosis. Front Immunol **7:**150.
12. **Vergne I, Fratti RA, Hill PJ, Chua J, Belisle J, Deretic V.** 2004. Mycobacterium tuberculosis phagosome maturation arrest: mycobacterial phosphatidylinositol analog phosphatidylinositol mannoside stimulates early endosomal fusion. Mol Biol Cell **15:**751-760.
13. **Flynn JL, Gideon HP, Mattila JT, Lin PL.** 2015. Immunology studies in non-human primate models of tuberculosis. Immunol Rev **264:**60-73.
14. **Cadena AM, Flynn JL, Fortune SM.** 2016. The Importance of First Impressions: Early Events in Mycobacterium tuberculosis Infection Influence Outcome. MBio **7:**e00342-00316.
15. **Coleman MT, Maiello P, Tomko J, Frye LJ, Fillmore D, Janssen C, Klein E, Lin PL.** 2014. Early Changes by (18)Fluorodeoxyglucose positron emission tomography coregistered with computed tomography predict outcome after Mycobacterium tuberculosis infection in cynomolgus macaques. Infect Immun **82:**2400-2404.
16. **Mattila JT, Ojo OO, Kepka-Lenhart D, Marino S, Kim JH, Eum SY, Via LE, Barry CE, 3rd, Klein E, Kirschner DE, Morris SM, Jr., Lin PL, Flynn JL.** 2013. Microenvironments in tuberculous granulomas are delineated by distinct populations of macrophage subsets and expression of nitric oxide synthase and arginase isoforms. J Immunol **191:**773-784.
17. **Gideon HP, Phuah J, Myers AJ, Bryson BD, Rodgers MA, Coleman MT, Maiello P, Rutledge T, Marino S, Fortune SM, Kirschner DE, Lin PL, Flynn JL.** 2015. Variability in tuberculosis granuloma T cell responses exists, but a balance of pro- and anti-inflammatory cytokines is associated with sterilization. PLoS Pathog **11:**e1004603.
18. **Flynn JL, Chan J, Lin PL.** 2011. Macrophages and control of granulomatous inflammation in tuberculosis. Mucosal Immunol **4:**271-278.
19. **Gordon S, Martinez FO.** 2010. Alternative activation of macrophages: mechanism and functions. Immunity **32:**593-604.
20. **Gordon S, Taylor PR.** 2005. Monocyte and macrophage heterogeneity. Nat Rev Immunol **5:**953-964.

21. **Biswas SK, Mantovani A.** 2010. Macrophage plasticity and interaction with lymphocyte subsets: cancer as a paradigm. Nat Immunol **11:**889-896.
22. **Martinez FO, Sica A, Mantovani A, Locati M.** 2008. Macrophage activation and polarization. Front Biosci **13:**453-461.
23. **Eum SY, Kong JH, Hong MS, Lee YJ, Kim JH, Hwang SH, Cho SN, Via LE, Barry CE, 3rd.** 2010. Neutrophils are the predominant infected phagocytic cells in the airways of patients with active pulmonary TB. Chest **137:**122-128.
24. **Lin PL, Ford CB, Coleman MT, Myers AJ, Gawande R, Ioerger T, Sacchettini J, Fortune SM, Flynn JL.** 2014. Sterilization of granulomas is common in active and latent tuberculosis despite within-host variability in bacterial killing. Nat Med **20:**75-79.
25. **Prevention CfDCa.** 2016. Tuberculosis (TB) Disease: Symptoms & Risk Factors.
26. **Prevention CfDCa.** 2016. How TB Spreads.
27. **Gideon HP, Flynn JL.** 2011. Latent tuberculosis: what the host "sees"? Immunol Res **50:**202-212.
28. **Ankrah AO, van der Werf TS, de Vries EF, Dierckx RA, Sathekge MM, Glaudemans AW.** 2016. PET/CT imaging of Mycobacterium tuberculosis infection. Clin Transl Imaging **4:**131-144.
29. **Zar HJ, Connell TG, Nicol M.** 2010. Diagnosis of pulmonary tuberculosis in children: new advances. Expert Rev Anti Infect Ther **8:**277-288.
30. **Pai M, Zwerling A, Menzies D.** 2008. Systematic review: T-cell-based assays for the diagnosis of latent tuberculosis infection: an update. Ann Intern Med **149:**177-184.
31. **Esmail H, Lai RP, Lesosky M, Wilkinson KA, Graham CM, Coussens AK, Oni T, Warwick JM, Said-Hartley Q, Koegelenberg CF, Walzl G, Flynn JL, Young DB, Barry Iii CE, O'Garra A, Wilkinson RJ.** 2016. Characterization of progressive HIV-associated tuberculosis using 2-deoxy-2-[18F]fluoro-D-glucose positron emission and computed tomography. Nat Med **22:**1090-1093.
32. **Kapoor V, McCook BM, Torok FS.** 2004. An introduction to PET-CT imaging. Radiographics **24:**523-543.
33. **Lin PL, Coleman T, Carney JP, Lopresti BJ, Tomko J, Fillmore D, Dartois V, Scanga C, Frye LJ, Janssen C, Klein E, Barry CE, 3rd, Flynn JL.** 2013. Radiologic responses in cynomolgous macaques for assessing tuberculosis chemotherapy regimens. Antimicrob Agents Chemother doi:10.1128/AAC.00277-13.
34. **Via LE, Schimel D, Weiner DM, Dartois V, Dayao E, Cai Y, Yoon YS, Dreher MR, Kastenmayer RJ, Laymon CM, Carny JE, Flynn JL, Herscovitch P, Barry CE, 3rd.** 2012. Infection dynamics and response to chemotherapy in a rabbit model of tuberculosis using [(1)(8)F]2-fluoro-deoxy-D-glucose positron emission tomography and computed tomography. Antimicrob Agents Chemother **56:**4391-4402.
35. **Lin PL, Rodgers M, Smith L, Bigbee M, Myers A, Bigbee C, Chiosea I, Capuano SV, Fuhrman C, Klein E, Flynn JL.** 2009. Quantitative comparison of active and latent tuberculosis in the cynomolgus macaque model. Infect Immun **77:**4631-4642.
36. **Shi L, Salamon H, Eugenin EA, Pine R, Cooper A, Gennaro ML.** 2015. Infection with Mycobacterium tuberculosis induces the Warburg effect in mouse lungs. Sci Rep **5:**18176.
37. **Macintyre AN, Rathmell JC.** 2013. Activated lymphocytes as a metabolic model for carcinogenesis. Cancer Metab **1:**5.
38. **Rius J, Guma M, Schachtrup C, Akassoglou K, Zinkernagel AS, Nizet V, Johnson RS, Haddad GG, Karin M.** 2008. NF-kappaB links innate immunity to the hypoxic response through transcriptional regulation of HIF-1alpha. Nature **453:**807-811.
39. **Imtiyaz HZ, Simon MC.** 2010. Hypoxia-inducible factors as essential regulators of inflammation. Curr Top Microbiol Immunol **345:**105-120.
40. **Werth N, Beerlage C, Rosenberger C, Yazdi AS, Edelmann M, Amr A, Bernhardt W, von Eiff C, Becker K, Schafer A, Peschel A, Kempf VA.** 2010. Activation of hypoxia inducible factor 1 is a general phenomenon in infections with human pathogens. PLoS One **5:**e11576.
41. **Peyssonnaux C, Datta V, Cramer T, Doedens A, Theodorakis EA, Gallo RL, Hurtado-Ziola N, Nizet V, Johnson RS.** 2005. HIF-1alpha expression regulates the bactericidal capacity of phagocytes. J Clin Invest **115:**1806-1815.
42. **Haeberle HA, Durrstein C, Rosenberger P, Hosakote YM, Kuhlicke J, Kempf VA, Garofalo RP, Eltzschig HK.** 2008. Oxygen-independent stabilization of hypoxia inducible factor (HIF)-1 during RSV infection. PLoS One **3:**e3352.

43. **Hwang, II, Watson IR, Der SD, Ohh M.** 2006. Loss of VHL confers hypoxia-inducible factor (HIF)-dependent resistance to vesicular stomatitis virus: role of HIF in antiviral response. J Virol **80:**10712-10723.
44. **Cramer T, Yamanishi Y, Clausen BE, Forster I, Pawlinski R, Mackman N, Haase VH, Jaenisch R, Corr M, Nizet V, Firestein GS, Gerber HP, Ferrara N, Johnson RS.** 2003. HIF-1alpha is essential for myeloid cell-mediated inflammation. Cell **112:**645-657.
45. **Belton M, Brilha S, Manavaki R, Mauri F, Nijran K, Hong YT, Patel NH, Dembek M, Tezera L, Green J, Moores R, Aigbirhio F, Al-Nahhas A, Fryer TD, Elkington PT, Friedland JS.** 2016. Hypoxia and tissue destruction in pulmonary TB. Thorax doi:10.1136/thoraxjnl-2015-207402.
46. **Dang EV, Barbi J, Yang HY, Jinasena D, Yu H, Zheng Y, Bordman Z, Fu J, Kim Y, Yen HR, Luo W, Zeller K, Shimoda L, Topalian SL, Semenza GL, Dang CV, Pardoll DM, Pan F.** 2011. Control of T(H)17/T(reg) balance by hypoxia-inducible factor 1. Cell **146:**772-784.
47. **Jantsch J, Chakravortty D, Turza N, Prechtel AT, Buchholz B, Gerlach RG, Volke M, Glasner J, Warnecke C, Wiesener MS, Eckardt KU, Steinkasserer A, Hensel M, Willam C.** 2008. Hypoxia and hypoxia-inducible factor-1 alpha modulate lipopolysaccharide-induced dendritic cell activation and function. J Immunol **180:**4697-4705.
48. **Zhuang H, Alavi A.** 2002. 18-fluorodeoxyglucose positron emission tomographic imaging in the detection and monitoring of infection and inflammation. Semin Nucl Med **32:**47-59.
49. **Matthies A, Hickeson M, Cuchiara A, Alavi A.** 2002. Dual time point 18F-FDG PET for the evaluation of pulmonary nodules. J Nucl Med **43:**871-875.
50. **Augustin R.** 2010. The protein family of glucose transport facilitators: It's not only about glucose after all. IUBMB Life **62:**315-333.
51. **Zhao FQ, Keating AF.** 2007. Functional properties and genomics of glucose transporters. Curr Genomics **8:**113-128.
52. **Illsley NP.** 2000. Glucose transporters in the human placenta. Placenta **21:**14-22.
53. **Orci L, Thorens B, Ravazzola M, Lodish HF.** 1989. Localization of the pancreatic beta cell glucose transporter to specific plasma membrane domains. Science **245:**295-297.
54. **Johnson JH, Newgard CB, Milburn JL, Lodish HF, Thorens B.** 1990. The high Km glucose transporter of islets of Langerhans is functionally similar to the low affinity transporter of liver and has an identical primary sequence. J Biol Chem **265:**6548-6551.
55. **Thorens B, Mueckler M.** 2010. Glucose transporters in the 21st Century. Am J Physiol Endocrinol Metab **298:**E141-145.
56. **Huang S, Czech MP.** 2007. The GLUT4 glucose transporter. Cell Metab **5:**237-252.
57. **Godoy A, Ulloa V, Rodriguez F, Reinicke K, Yanez AJ, Garcia Mde L, Medina RA, Carrasco M, Barberis S, Castro T, Martinez F, Koch X, Vera JC, Poblete MT, Figueroa CD, Peruzzo B, Perez F, Nualart F.** 2006. Differential subcellular distribution of glucose transporters GLUT1-6 and GLUT9 in human cancer: ultrastructural localization of GLUT1 and GLUT5 in breast tumor tissues. J Cell Physiol **207:**614-627.
58. **Lisinski I, Schurmann A, Joost HG, Cushman SW, Al-Hasani H.** 2001. Targeting of GLUT6 (formerly GLUT9) and GLUT8 in rat adipose cells. Biochem J **358:**517-522.
59. **Masin M, Vazquez J, Rossi S, Groeneveld S, Samson N, Schwalie PC, Deplancke B, Frawley LE, Gouttenoire J, Moradpour D, Oliver TG, Meylan E.** 2014. GLUT3 is induced during epithelial-mesenchymal transition and promotes tumor cell proliferation in non-small cell lung cancer. Cancer Metab **2:**11.
60. **Chung JK, Lee YJ, Kim SK, Jeong JM, Lee DS, Lee MC.** 2004. Comparison of [18F]fluorodeoxyglucose uptake with glucose transporter-1 expression and proliferation rate in human glioma and non-small-cell lung cancer. Nucl Med Commun **25:**11-17.
61. **Organization WH.** 2017. The top 10 causes of death.
62. **Greenberg J.** January 11, 2017 2017. Does tuberculosis top HIV/AIDS as the deadlier disease? http://www.politifact.com/global-news/statements/2017/jan/11/nick-seymour/tuberculosis-might-top-hivaids-deadliest-infectiou/. Accessed
63. **Fu Y, Maianu L, Melbert BR, Garvey WT.** 2004. Facilitative glucose transporter gene expression in human lymphocytes, monocytes, and macrophages: a role for GLUT isoforms 1, 3, and 5 in the immune response and foam cell formation. Blood Cells Mol Dis **32:**182-190.

64. **Kalsi KK, Baker EH, Medina RA, Rice S, Wood DM, Ratoff JC, Philips BJ, Baines DL.** 2008. Apical and basolateral localisation of GLUT2 transporters in human lung epithelial cells. Pflugers Arch **456:**991-1003.
65. **Ozaki T, Nakahira S, Tani K, Ogushi F, Yasuoka S, Ogura T.** 1992. Differential cell analysis in bronchoalveolar lavage fluid from pulmonary lesions of patients with tuberculosis. Chest **102:**54-59.
66. **Law K, Weiden M, Harkin T, Tchou-Wong K, Chi C, Rom WN.** 1996. Increased release of interleukin-1 beta, interleukin-6, and tumor necrosis factor-alpha by bronchoalveolar cells lavaged from involved sites in pulmonary tuberculosis. Am J Respir Crit Care Med **153:**799-804.
67. **Mattila JT, Maiello P, Sun T, Via LE, Flynn JL.** 2015. Granzyme B-expressing neutrophils correlate with bacterial load in granulomas from Mycobacterium tuberculosis-infected cynomolgus macaques. Cell Microbiol **17:**1085-1097.
68. **Shao Y, Wellman TL, Lounsbury KM, Zhao FQ.** 2014. Differential regulation of GLUT1 and GLUT8 expression by hypoxia in mammary epithelial cells. Am J Physiol Regul Integr Comp Physiol **307:**R237-247.